

Response to Reviewers' comments (Manuscript Ref. NO.: acp-2017-120)

We would like to thank the reviewers for the thoughtful comments. We have carefully studied these comments and made the corrections. The quality of this manuscript has been greatly improved due to the valuable suggestions. The detailed responses to specific questions are presented in the following.

Reviewer #1:

Overall Comment

This paper presents an interesting contribution aiming at the development of new numerical model of dust (photo)chemistry. It describes in some detail the different key process that are implemented. Clearly, the use of surface photochemistry is a novel and valuable contribution. However, a few aspects of this modelling studies are raising a few important questions.

Comment 1: The partitioning between the gas and condensed phase are treated in a similar way, despite being fundamentally different in nature. For a solid surface, the adsorption and desorption processes do follow a different formalism, typically through a Langmuir-Hinshelwood formalism which takes into account a given number of adsorption sites. The consequences is that adsorption decreases with time or increasing concentration, while here it is simulated in a constant way with time. how can you justify such an assumption? Also products such as sulfate are probably staying on the surface, thereby also using adsorption sites i.e., poisoning the surface. How would your model change if you implement such time/concentration dependence?

Response: We assumed that the gas-particle partitioning onto dust is operated by an absorption process (Eq. 7) by several reasons (see section 3.2.1). First, unlike pure metal oxide which is governed by the adsorptive partitioning, the composition of authentic mineral dust such as Arizona Test Dust (ATD) is complex. The fresh ATD contains inorganic salts that are hygroscopic and form the water film above efflorescence relative humidity or deliquescence relative humidity. Second, the partitioning process is dynamic due to the formation of various hygroscopic salts of sulfate and nitrate due to the reaction of alkaline carbonates and metal oxides with inorganic acids (sulfuric acid and nitric acid). Third, the sulfate formation in our study increased as increasing humidity due to the dissolution of tracers into the water layer (see section 3.2.1). If partitioning is processed by the adsorptive mode, water molecules compete for the site with tracers and reduce partitioning of tracers (Cwiertny et al., 2008). The amount of the surface water on dust particles, which was measured using FTIR (submitted in the other journal), was multi-layered.

Comment 2: Why having chosen to simulate deliquesced sea-salt and dust in the same code? What is the link between both objects/themes? Can you justify such a choice? Also the text mentions sea-salt and the partitioning process is described for aqueous sulfuric acid particles. Please harmonize the different part of your manuscript.

Response: We have never mentioned about the deliquesced sea-salt in this study. For the formation of sulfuric acid in inorganic salted aqueous aerosol ($\text{SO}_4^{2-}\text{-NH}_4^+\text{-H}_2\text{O}$ system) (Section 3.1.3), we employed the aqueous phase kinetic reactions previously reported in literatures (Lee, 1984; Strehlow and Wagner, 1982; Gratzel et al., 1970; Graedel and Weschler, 1981; Treinin and Hayon, 1970; Lee and Lind, 1986; Damschen and Martin, 1983; Liang and Jacobson, 1999; Hoyle et al., 2016).

Comment 3: The characteristic time for adsorption is very different between aqueous and dust particles. Is this physically justified, bearing in mind that those processes are mostly related to gas phase and aerosols properties.

Response: The characteristic time of the uptake process of gas into aqueous phase or dust phase is calculated for gas-phase diffusion, liquid phase diffusion, establishing equilibrium at the interface and the reactions in gas, aqueous, and dust phases (Finlayson-Pitts and Pitts Jr, 1999). Table S2 has been added to supporting information in revised manuscript.

Table S2. The calculation of the characteristic time of the major processes and reactions

Type of process	Characteristic time	Aqueous phase system	Dust system
r : the particle radius D_g : diffusion coefficient in gas D_l : diffusion coefficient in aqueous phase H : Henry's constant α : the mass accommodation coefficient (0.5) u_{av} is the mean thermal speed.		$r = 50 \text{ nm}$ $k_{\text{SO}_2,g} = 1 \times 10^{-12} \text{ s}^{-1} \text{ molecule}^{-1} \text{ cc}$ $[\text{OH}] = 1 \times 10^6 \text{ molecules cc}^{-1}$ $k_{\text{HSO}_3} = 3 \times 10^{-3} \text{ s}^{-1} \text{ molecule}^{-1} \text{ cc}$ $[\text{OH}]_{\text{aq}} = 0.1 \text{ molecules cc}^{-1}$	$r = 350 \text{ nm}$ (average) $r_{\text{dust,aq}}$: the average thickness of the water layer on dust particles (40 nm) $k_{\text{SO}_2,g} = 1 \times 10^{-12} \text{ s}^{-1} \text{ molecule}^{-1} \text{ cc}$ $[\text{OH}] = 1 \times 10^6 \text{ molecules cc}^{-1}$ $k_{\text{SO}_2,\text{dust}} = 1 \times 10^{-12} \text{ s}^{-1} \text{ molecule}^{-1} \text{ cc}$ $[\text{OH}]_{\text{aq}} = 2 \times 10^9 \text{ molecules cc}^{-1}$
Gas diffusion	$\frac{r^2}{\pi^2 D_g}$	$2.4 \times 10^{-11} \text{ s}$	$2.1 \times 10^{-10} \text{ s}$
Diffusion in aqueous phase	$\frac{r_{\text{aq}}^2}{\pi^2 D_l}$	$1.9 \times 10^{-7} \text{ s}$	
Diffusion in the water layer on dust	$\frac{r_{\text{dust,aq}}^2}{\pi^2 D_l}$		$1.2 \times 10^{-7} \text{ s}$
Equilibrium between gas and particle	$D_l \left(\frac{4HRT}{\alpha u_{av}} \right)^2$	$7.1 \times 10^{-10} \text{ s}$	$7.1 \times 10^{-10} \text{ s}$
Reaction in gas phase	$\frac{1}{[\text{OH}] k_{\text{SO}_2,g}}$	$1 \times 10^6 \text{ s}$	$1 \times 10^6 \text{ s}$
Reaction in aqueous phase	$\frac{1}{[\text{OH}]_{\text{aq}} k_{\text{HSO}_3,\text{aq}}}$	$2 \times 10^3 \text{ s}$	
Reaction in dust phase	$\frac{1}{[\text{OH}]_{\text{dust}} k_{\text{SO}_2,\text{dust}}}$		$5 \times 10^2 \text{ s}$

For both the aqueous system and the dust system, the characteristic time of all reactions in gas and particles are much greater than diffusion in gas or particle phases and equilibrium processes (partitioning and dissociation of acids). Thus, the reactions of chemical species are not affected by the time reached to equilibrium or diffusion processes. In the model, both absorption and desorption rates of chemical species were set to much faster than their reaction rates in all three phase (last paragraph in Section 3.1.2). Furthermore, the time of diffusion in the liquid phase is longer than both gas diffusion and the time for reaching to equilibrium as shown in Table S2.

Comment 4: Too many rate constants are estimated without any justification. Please justify and explain your estimations.

Response: Most of the rate constants shown in Table 3 were estimated using the indoor chamber data obtained in the previous study (Park and Jang, 2016). The rate constants of R10 (electron-hole production) and R11 (recombination of electron-hole) in the manuscript is estimated using Eq. 10 (photoactivation rate, J_{ATD}) in the manuscript (Section 3.2.3). The rate constant of R13 (reaction of SO_2 with dust-phase OH radicals) is set to the same reaction rate constant for the reaction of SO_2 with OH radicals in gas phase. Without sunlight, autoxidation of SO_2 (R9) is dominant in dust phase and its rate constant was obtained from indoor chamber data under various humidity conditions (Exp. D1-D3 in Table 1). With sunlight, the photochemical reaction is the major source for sulfate production. Using the same approach with autoxidation, the rate constant of R12 was estimated under different humidity conditions. Also, the rate constants of R14 (heterogeneous autoxidation of SO_2 in the presence of ozone) and R15 (heterogeneous oxidation of O_3) were estimated using experiments D4 and L5 in Table 1, respectively. The rate constants of R18 (heterogeneous autoxidation of NO_2) and R19 (heterogeneous photocatalytic oxidation of NO_2) were estimated using experiments D5 and L7 in Table 1, respectively.

Comment 5: The agreement with the chamber data has to be described in a more quantitative way. By looking at the figures, one may have the impression that the agreement is not as good as described in the text.

Response: We agree with the reviewer. After carefully searching the errors, we found that mistakes in the estimation of the aerosol water content and aerosol acidity due to the incorrect input parameter for the titration of sulfuric acid with ammonia. The FS value, a numeric number to dynamically represent the composition of the sulfate-ammonium aerosol system, ranges from 0.34 (ammonium sulfate) to 1.0 (sulfuric acid). In the previous simulation, FS was computed sometimes at out of range due to the incorrect input of ammonia data. By the correction of this error, the model prediction in Fig. 3 were improved. In addition to the correction of input errors, we found some contamination in the NO_2 tank by nitric acid for the experiments with NO_2 (11/26/2015, 11/05/2016 and 11/22/2016). We conducted additional experiments with the new NO_x tank (Table 2 in the revised manuscript) and applied these new data to model evaluations (Figure 4 and Table 2 in the revised manuscript). The simulation of SO_2 oxidation in the presence of NO_2 was much improved.

Reviewer #2:

Overall Comment

This manuscript represents a model for evaluating the importance of dust in sulfate formation, particularly in adding the kinetics and mechanism of heterogeneous photocatalytic reactions of SO₂ on mineral dust in the model. It is essential to consider the photooxidation of SO₂ in order to improve the accuracy of sulfate formation modeled in the atmosphere. Therefore, this study is of substantial interest. However, some major points should be carefully considered before it is published.

Comment 1: The indoor chamber data shows that, in the absence of ATD particles, [SO₄²⁻]_T at 55% RH is two times larger than that at 19% RH (Table 1 L1A, B and C), but when RH increases to 80%, the enhancement of [SO₄²⁻]_T is not distinct. Additionally, in the presence of ATD particles, [SO₄²⁻]_T is unexpectedly lower than that in the absence of ATD at 55% RH (Table 1 L3 and L1B), contrary to that at 80% RH (Table 1 L4 and L1C). However, these observations are not discussed in the manuscript and shown in the model.

Response: The data of Table 1 is obtained and reorganized from previous study (Park and Jang, 2016). In Table 1, [SO₄²⁻]_T is the observation of total sulfate concentration which is dependent of the initial SO₂, RH, dust concentration and the duration of the experiment. Figure 2 illustrates the impact of RH on uptake coefficient of SO₂ with and without UV light. The uptake coefficients which were determined using fitting the kinetic model to experimental data agree with those reported in the previous work by Park and Jang (2016). Exp. L1A, L1B and L1C in Table 1 were for SO₂ oxidation without dust particles and removed in the revised manuscript because they were not used for this paper.

Comment 2: In addition to react with SO₂ and NO₂, OH radicals produced on the surface of particles under UV conditions can undergo heterogeneous reaction with particles as well as self-reactions, resulting in the significant decrease of OH radicals participate in the oxidation of SO₂ and NO₂, and subsequently overestimating sulfate and nitrate formation in the model. Furthermore, in addition to compete OH radicals with SO₂, the presence of NO₂ can also react with SO₂ on the surface of particles to promote sulfate formation at high RHs as like in aqueous phase. However, these mechanisms were not considered in dust phase in the model (Table S1).

Response: In our model, the apparent rate constant of the formation of the dust-phase OH radicals is estimated using indoor chamber data. The synergistic effect of NO₂ on sulfate formation under UV light is explained by the HONO production through the reaction of NO₂ with electrons or holes in dust phase (R16). HONO will then be decomposed via photolysis to form OH radicals (R17).

Comment 3: In Figure 3, it seems that modeled results are not in agreement with experimental observations at scenarios (a) without ATD particles and (b) low loadings of dust particles,

especially for time-changing trends, meaning that the gas and aqueous phase reaction of SO₂ may be not well considered in the model. The authors should give explanations or speculations for this discrepancy in the manuscript.

Response: Please also fine the response to comment 5 from reviewer 1. We agree with the reviewer's comment. The estimation of aerosol water content was incorrect in the previous simulation due to the wrong input of aerosol acidity. By correcting this error, the model simulation of sulfate and nitrate has been greatly improved (Figs 3 and 4).

Comment 4: The authors estimated gas-particle partitioning constant of NO₂, K_{d,NO_2} , based on the relationship between the Henry's law constants of NO₂ and SO₂ (Eq. 15), but K_{d,O_3} is obtained from literature results (Eq. 14). Is it reasonable to estimate K_{d,NO_2} according to Eq. (15)? And why K_{d,NO_2} and K_{d,O_3} are set based on different method since previous studies have investigated the heterogeneous reaction of NO₂ on mineral dust as well? Moreover, in Section 3.2.1 the authors considered the influence of RH on K_{d,SO_2} , however, the expression of K_{d,NO_2} and K_{d,O_3} . The concentration otration of which is also closely related sulfate formation in the model, was not shown as a function of RH.

Response: The estimation of the gas-dust partitioning coefficient of ozone is scaled using the gas-dust partitioning of SO₂ reported in literature and the ratio of Henry' constant of SO₂ to ozone, similar to NO₂ (the first sentence of Sect. 3.3.1). The partitioning process of tracers on the dust phase is treated as absorption and desorption process (please also see the response to the Comment 1 of Referee 1). The absorption process is influenced by the aerosol water content. Thus, we assume that relative ratio of the Henry's law constants normalized by constant of SO₂, is applicable to estimate the gas-dust partitioning coefficient of tracers. For example, the Henry's law constants of both NO₂ and ozone are $1.2 \times 10^{-2} \text{ mol L}^{-1} \text{ atm}^{-1}$ at 298K (Chameides, 1984) and they are 100 times smaller than that of SO₂ ($1.2 \text{ mol L}^{-1} \text{ atm}^{-1}$)(Chameides, 1984). All gas-dust partitioning coefficients are dependent of humidity (see Eq. 7, 14, and 15).

Minor Comments:

Comment 5: Page 4 Line 27 "The detail description" should be "The detailed description"

Response: It was corrected.

Comment 6: Page 4 Line 21 The indoor chamber data of this study was obtained from our recent laboratory study (Park and Jang, 2016), however, $[SO_4^{2-}]_T$ values shown in Table 1 is different with Park and Jang (2016) reported. For example, Table 1 D1, L1 B and L8 in the manuscript corresponding to Table 1 D1, L1D and L8 in Park and Jang (2016), respectively.

Response: The model simulation was performed against the data points over the course of the chamber experiment. The $[SO_4^{2-}]_T$ values in Table 1 are sourced from the last data point in time

for each chamber experiment that previously reported by Park and Jang (2016). In order to drive the model parameters, the outliers were removed for some data sets. When data was available, different simulation time were used for some data sets. Data sets L1A, L1B, and L1C for SO₂ oxidation without dust particles were not used in this study. Thus, they were removed from Table 1. For the heterogeneous autoxidation of SO₂ in the presence of ozone, the newly produced indoor chamber data (Data D4 in Table 1) was used to drive the AMAR model. As described in the response to comment 5 of reviewer 1, we found the contamination of the NO₂ tank by nitric acid. Thus, we removed data sets L6 and L7 from Table 1. To insure the quality of the data used for the model, the new outdoor chamber data sets were produced for heterogeneous oxidation of SO₂ in the presence of NO_x and they were applied to model development: data on 04/14/2017 in Table 2 for driving model parameters and two data sets on 04/25/2017 for model evaluation.

Comment 7: Page 7 Line 19 and 21 “SO₄²⁻-NH₄⁺-H₂O” should be “SO₄²⁻-NH₄⁺-H₂O”.

Response: This has been done.

Comment 8: Page 11 Line 17 Give more detailed description about k_{autoo} and $k_{\text{OH}, \text{O}_2}$ derived from the indoor chamber data.

Response: In the dark condition, the formation of sulfate is mainly from the autoxidation of SO₂. By fitting the predicted sulfate concentration to the experimental observation (D1- D3 in Table 1), the SO₂ autoxidation reaction rate constant ($k_{\text{auto}}, \text{s}^{-1}$) is semiempirically determined. Also see the last third sentence of Sect. 3.2.2. Using same approach, $k_{\text{OH}, \text{O}_2}$ is first estimated using indoor chamber data (L1-L3 in Table 1) at RH 20%, 55% and 80% and then regressed against RH. Also see the last sentence of the second paragraph of Sect. 3.2.3.

Comment 9: Page 14 Line 21 “L7 and L8 in Table 1” should be “L6 and L7 in Table 1”.

Response: It was corrected. Thank you very much for your comments.

Reference

- Cwiertny, D. M., Young, M. A., and Grassian, V. H.: Chemistry and photochemistry of mineral dust aerosol, *Annu Rev Phys Chem*, 59, 27-51, 10.1146/annurev.physchem.59.032607.093630, 2008.
- Damschen, D. E., and Martin, L. R.: Aqueous aerosol oxidation of nitrous acid by O₂, O₃ and H₂O₂, *Atmospheric Environment* (1967), 17, 2005-2011, 1983.
- Finlayson-Pitts, B. J., and Pitts Jr, J. N.: Chemistry of the upper and lower atmosphere: theory, experiments, and applications, Academic press, 1999.
- Graedel, T., and Weschler, C.: Chemistry within aqueous atmospheric aerosols and raindrops, *Rev Geophys*, 19, 505-539, 1981.
- Grätzel, M., Taniguchi, S., and Henglein, A.: Pulsradiolytische Untersuchung der NO-Oxydation und des Gleichgewichts $\text{N}_2\text{O}_3 \rightleftharpoons \text{NO} + \text{NO}_2$ in wäßriger Lösung, *Berichte der Bunsengesellschaft für physikalische Chemie*, 74, 488-492, 1970.
- Hoyle, C. R., Fuchs, C., Jarvinen, E., Saathoff, H., Dias, A., El Haddad, I., Gysel, M., Coburn, S. C., Trostl, J., Bernhammer, A. K., Bianchi, F., Breitenlechner, M., Corbin, J. C., Craven, J., Donahue, N. M., Duplissy, J., Ehrhart, S., Frege, C., Gordon, H., Hoppel, N., Heinritzi, M., Kristensen, T. B., Molteni, U., Niehman, L., Pinterich, T., Prevot, A. S. H., Simon, M., Slowik, J. G., Steiner, G., Tome, A., Vogel, A. L., Volkamer, R., Wagner, A. C., Wagner, R., Wexler, A. S., Williamson, C., Winkler, P. M., Yan, C., Amorim, A., Dommen, J., Curtius, J., Gallagher, M. W., Flagan, R. C., Hansel, A., Kirkby, J., Kulmala, M., Mohler, O., Stratmann, F., Worsnop, D. R., and Baltensperger, U.: Aqueous phase oxidation of sulphur dioxide by ozone in cloud droplets, *Atmos Chem Phys*, 16, 1693-1712, 10.5194/acp-16-1693-2016, 2016.
- Krueger, B. J., Grassian, V. H., Laskin, A., and Cowin, J. P.: The transformation of solid atmospheric particles into liquid droplets through heterogeneous chemistry: Laboratory insights into the processing of calcium containing mineral dust aerosol in the troposphere, *Geophys Res Lett*, 30, Art. 1148 10.1029/2002gl016563, 2003.
- Lee, Y.-N.: Atmospheric aqueous-phase reactions of nitrogen species, Brookhaven National Lab., Upton, NY (USA), 1984.
- Lee, Y. N., and Lind, J. A.: Kinetics of aqueous-phase oxidation of nitrogen (III) by hydrogen peroxide, *Journal of Geophysical Research: Atmospheres*, 91, 2793-2800, 1986.
- Liang, J. Y., and Jacobson, M. Z.: A study of sulfur dioxide oxidation pathways over a range of liquid water contents, pH values, and temperatures, *J Geophys Res-Atmos*, 104, 13749-13769, Doi 10.1029/1999jd900097, 1999.
- Liu, Y. J., Zhu, T., Zhao, D. F., and Zhang, Z. F.: Investigation of the hygroscopic properties of Ca(NO₃)₂ and internally mixed Ca(NO₃)₂/CaCO₃ particles by micro-Raman spectrometry, *Atmos Chem Phys*, 8, 7205-7215, 2008.
- Park, J., and Jang, M.: Heterogeneous photooxidation of sulfur dioxide in the presence of airborne mineral dust particles, *RSC Advances*, 6, 58617-58627, 2016.
- Strehlow, H., and Wagner, I.: Flash photolysis in aqueous nitrite solutions, *Zeitschrift für Physikalische Chemie*, 132, 151-160, 1982.
- Treinin, A., and Hayon, E.: Absorption spectra and reaction kinetics of NO₂, N₂O₃, and N₂O₄ in aqueous solution, *J Am Chem Soc*, 92, 5821-5828, 1970.

Modelling Atmospheric Mineral Aerosol Chemistry to Predict Heterogeneous Photooxidation of SO₂

Zeichen Yu, Myoseon Jang, and Jiyeon Park

5 P.O. Box 116450, Department of Environmental Engineering Sciences, Engineering School of Sustainable
Infrastructure and Environment, University of Florida, Gainesville, FL, USA, 32611
Corresponding author: Myoseon Jang, mjang@ufl.edu

Abstract.

The photocatalytic ability of airborne mineral dust particles is known to heterogeneously
10 promote SO₂ oxidation, but prediction of this phenomenon is not fully taken into account by
current models. In this study, the Atmospheric Mineral Aerosol Reaction (AMAR) model was
developed to capture the influence of air-suspended mineral dust particles on sulfate formation in
various environments. In the model, SO₂ oxidation proceeds in three phases including the gas
phase, the inorganic-salted aqueous phase (non-dust phase), and the dust phase. Dust chemistry
15 is described as the ~~adsorption~~absorption-desorption kinetics (gas-particle partitioning) of SO₂ and
NO_x. The reaction of ~~adsorbed~~absorbed SO₂ on dust particles occurs *via* two major paths:
autoxidation of SO₂ in open air and photocatalytic mechanisms under UV light. The kinetic
mechanism of autoxidation was first leveraged using controlled indoor chamber data in the
presence of Arizona Test Dust (ATD) particles without UV light, and then extended to
20 photochemistry. With UV light, SO₂ photooxidation was promoted by surface oxidants (OH
radicals) that are generated *via* the photocatalysis of semiconducting metal oxides (electron-hole
theory) of ATD particles. This photocatalytic rate constant was derived from the integration of the
combinational product of the dust absorbance spectrum and wave-dependent actinic flux for the
full range of wavelengths of the light source. The predicted concentrations of sulfate and nitrate
25 using the AMAR model agreed well with outdoor chamber data that were produced under natural
sunlight. For seven consecutive hours of photooxidation of SO₂ in an outdoor chamber, dust
chemistry at the low NO_x level was attributed to ~~70~~55% of total sulfate (~~5660~~ ppb SO₂, 290 µg m⁻³
ATD, and NO_x less than 5 ppb). At high NO_x (>50 ppb of NO_x with low hydrocarbons), sulfate
formation was also greatly promoted by dust chemistry, but it was suppressed by the competition
30 between NO₂ and SO₂ that both consume the dust-surface oxidants (OH radicals or ozone). The

AMAR model, derived in this study with ATD particles, will provide a platform for predicting sulfate formation in the presence of authentic dust particles (e.g. Gobi and Saharan dust).

1 Introduction

The surface of mineral dust particles is able to act as sink for various atmospheric trace gases such as sulfur dioxide (SO₂), nitrogen oxides (NO_x, e.g. NO and NO₂), and ozone (O₃). Among trace gases, SO₂ has received much attention because heterogeneous oxidation of SO₂ produces nonvolatile sulfuric acid, which is readily involved in the acidification of particles or the reaction with dust constituents such as alkaline metals (K⁺, Na⁺) or metal oxides (e.g. α-Al₂O₃ and Fe₂O₃). Such modification of the chemical composition of dust particles can influence the hygroscopic properties of mineral dust, which is essential to activate cloud condensation nucleation (Krueger et al., 2003; Zhang and Chan, 2002; Vlasenko et al., 2006; Liu et al., 2008; Tang et al., 2016).

Metal oxides (e.g. TiO₂ and Al₂O₃) have frequently been used in many laboratories to study the key role of mineral dust in the heterogeneous oxidation of SO₂ (Goodman et al., 2001; Usher et al., 2002; Zhang et al., 2006). However, these laboratory studies have been limited to a certain type of metal oxide and autoxidation of SO₂ without a light source. To date, only a few studies have attempted to study the photocatalytic characteristics of mineral dust in the oxidation of SO₂ and NO_x. For example, as noted by Park and Jang (2016), the reactive uptake coefficient ($\gamma_{SO_4^{2-}}$) of SO₂ in the presence of dry Arizona Test Dust (ATD) particles under UV light was one order of magnitude higher (1.16×10^{-6} using an indoor chamber with a light mix of UV-A and UV-B light) than that from autoxidation (1.15×10^{-7}) without a light source. Using an aerosol flow tube, Dupart et al. (2014) observed that the uptake rate of NO₂ by ATD dust particles was significantly enhanced (by four times) under UV-A irradiation compared to dark conditions. Field observations have also reported the promotion of SO₂ photooxidation in the presence of mineral dust. For instance, near Beijing, China (ground-based campaign in 2009), and in Lyon, France (remote-sensing campaign in 2010), Dupart et al. (2012) found that mineral dust was a source of OH radicals under UV radiation that promoted sulfate formation.

Semiconducting metal oxides (e.g. α-Al₂O₃, α-Fe₂O₃, and TiO₂) act as a photocatalyst in mineral dust particles that can yield electron (e⁻_{cb})–hole (h⁺_{vb}) pairs, and that they are involved in the production of strong oxidizers, such as superoxide radical anions (O₂⁻) and OH radicals (Linsebigler et al., 1995; Hoffmann et al., 1995; Thompson and Yates, 2006; Cwiertny et al., 2008; Chen et al., 2012; Dupart et al., 2014; Colmenares and Luque, 2014). These oxidizers enable

rapid oxidation of adsorbed SO₂ and NO_x on the surface of mineral dust particles. For example, using transmission FTIR spectroscopy and X-ray photoelectron spectroscopy, Nanayakkara et al. (2012) observed the oxidation of SO₂ by the photo-catalytically generated OH radicals in the presence of titanium oxide particles. The heterogeneous formation of sulfate and nitrate can be highly variable and dependent on the chemical characteristics of dust aerosol (Gankanda et al., 2016). Authentic mineral dust particles differ from pure metal oxides in chemical composition. For example, Wagner et al. (2012) reported that the content of metal oxides in Saharan dust samples from Burkina Faso includes 14% Al₂O₃, 8.4% Fe₂O₃, and 1.2% TiO₂.

Most research on dust photochemistry has been limited to qualitative studies and lacks kinetic mechanisms that are linked to a predictive model. The typical wave-dependent photolysis of gas-phase trace gases has long been subject to atmospheric photochemistry. This photolysis rate is a first-order reaction and is calculated *via* the coupling actinic flux (the quantity of photons) with the characteristics (cross section area and quantum yield) of a light-absorbing molecule (McNaught and Wilkinson, 1997). In order to model dust photochemistry, the integration of wavelength-dependent actinic flux with photocatalytic activity of mineral dust is needed.

In addition to sunlight intensity, humidity also influences heterogeneous dust chemistry. Humidity governs particle water content, which influences the gas-dust sorption process of trace gases (Navea et al., 2010) and the formation of dust-phase oxidants. Huang et al. (2015) found that the $\gamma_{SO_4^{2-}}$ of SO₂ autooxidation in ATD particles increased by 142% because of the relative humidity (RH) changed from 15% to 90%. In the presence of UV light, the particle water content can act as an acceptor for h^+_{vb} and produce surface OH radicals, promoting heterogeneous photochemistry of SO₂ on mineral dust. In the presence of UV light, Shang et al. (2010) reported that sulfate production on the surface of TiO₂ increased by five times because of the increase of RH from 20% to 80%. Park and Jang (2016) also reported the exponential increase in $\gamma_{SO_4^{2-}}$ as the RH increased from 20% to 80% for both autooxidation and photooxidation of SO₂ in the presence of ATD particles. A few studies have attempted to simulate sulfate formation in the presence of mineral dust at regional scales using laboratory-generated kinetic parameters (Tang et al., 2004; Li and Han, 2010; Dong et al., 2016). However, $\gamma_{SO_4^{2-}}$ applied to the regional simulations originated from pure and dry metal oxides without UV light, and thus will differ from those of ambient dust exposed to natural sunlight. It is expected that the typical regional simulations during dust events might underestimate the formation of sulfate.

In this study, the Atmospheric Mineral Aerosol Reaction (AMAR) model was developed to predict atmospheric oxidation of trace gases such as SO₂ and NO₂ under ambient conditions. The kinetic mechanisms of dust-driven photochemistry, including autoxidation and photooxidation of SO₂, was newly established in the model. The rate constant of dust photoactivation, which forms electron-hole pairs and sources dust-driven oxidants, was integrated into the model. The influence of meteorological variables, such as humidity, temperature and sunlight, on SO₂ oxidation was investigated using the resulting AMAR model. The model also addresses the kinetic mechanism to simulate how atmospheric major pollutants such as NO_x and ozone are engaged in the oxidation of SO₂ in the presence of airborne dust particles. For environmental scenarios, the model was applied for polluted urban conditions (e.g. hydrocarbon ppbC/NO_x ppb < 5) and low NO_x conditions (e.g. hydrocarbon ppbC/NO_x ppb > 5). The reaction rate constants for both autoxidation and photocatalytic reactions of SO₂ were obtained through the simulation of indoor chamber data, which were previously generated under various meteorological and environmental conditions (Park and Jang, 2016). The suitability of the resulting AMAR model was tested against sulfate formation in a large outdoor smog chamber at the University of Florida Atmospheric Photochemical Outdoor Reactor (UF-APHOR) under natural sunlight. The AMAR model of this study will vastly improve the accuracy of the prediction of sulfate and nitrate formation in regional and global scales where dust emission is influential.

2 Experimental section

2.1 Chamber experiments

The indoor chamber data of this study was obtained from the recent laboratory study by Park and Jang (2016) to determine the kinetic rate constants that are needed to develop the AMAR model. The indoor chamber operation has been reported previously (Park and Jang 2016) (Also see Sect. S1). The indoor chamber data are listed in Table 1. The outdoor chamber experiments were performed in the UF-APHOR dual chambers (52 m³ for each chamber) to test the suitability of AMAR model to ambient condition. The light irradiation of the indoor-UV light and the sunlight are shown in Fig. S1. The detailed description of the operation of outdoor chamber are also described in Sect. S1. The outdoor experimental condition for SO₂ heterogeneous reaction in the presence of mineral dust particles are listed in Table 2.

2.2 Light absorption of ATD particles

The absorbance spectrum of ATD particles was measured to develop the reaction rate constants in the kinetic model. The detailed procedure for light absorption measurement of particle samples can be found in the previous study (Zhong and Jang, 2011). The particle size distribution of ATD is shown in Fig. S2. The suspended dust particles were sampled on a Teflon coated glass fiber filter for 20 minutes. The masses difference of dust sample was measured using a microbalance (MX5, Mettler Toledo, Columbus, OH). The light absorbance of the dust filter sample (Abs_{ATD}) was measured using a Perkin–Elmer Lambda 35 UV–visible spectrophotometer equipped with a Labsphere RSA–PE–20 diffuse–reflectance accessory. The absorbance spectrum was normalized by particle mass and calculated to mass absorbance cross section (See Sect. S1 in Supporting Information). The resulting absorbance cross section and quantum yield of ATD dust are shown in Fig. S3.

3 AMAR model description

The overall schematic of the AMAR model is shown in Fig 1. In the model, the total sulfate mass concentration ($[SO_4^{2-}]_T$, $\mu\text{g m}^{-3}$) is predicted from the reactions in three phases: the sulfate formed in the gas phase ($[SO_4^{2-}]_{\text{gas}}$, $\mu\text{g m}^{-3}$), the sulfate from the aqueous phase ($[SO_4^{2-}]_{\text{aq}}$, $\mu\text{g m}^{-3}$) and the sulfate from dust–driven chemistry ($[SO_4^{2-}]_{\text{dust}}$, $\mu\text{g m}^{-3}$). The key components of the model consist of the partitioning process and the kinetic mechanisms in three phases.

(1) The gaseous inorganic species (e.g. SO_2 , NO_x and ozone) are partitioned onto both inorganic–salt (sulfuric acid and its salts) seeded aqueous particles and mineral dust particles. The gas–particle partitioning processes were treated by the ~~adsorption~~absorption–desorption kinetic mechanism.

(2) SO_2 oxidation in the gas phase is simulated using mechanisms previously reported in the literature (Byun and Schere, 2006; Sarwar et al., 2013; Sarwar et al., 2014; Binkowski and Roselle, 2003) (Table. S1).

(3) The partitioned SO_2 is heterogeneously oxidized in the inorganic–salt seeded aqueous phase based on the previously reported mechanisms (Liang and Jacobson, 1999).

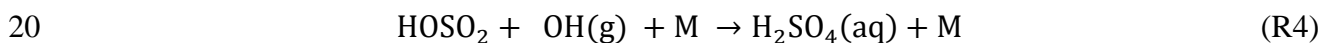
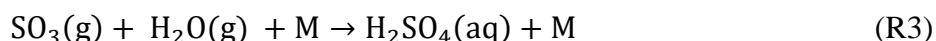
(4) The formation of sulfate ($[\text{SO}_4^{2-}]_{\text{dust}}$) in the dust phase is approached using two kinetic sub-modules: the production of sulfate ($[\text{SO}_4^{2-}]_{\text{auto}}$, $\mu\text{g m}^{-3}$) by autooxidation in open air and sulfate formation ($[\text{SO}_4^{2-}]_{\text{photo}}$, $\mu\text{g m}^{-3}$) by photocatalytic reactions.

The rate constants associated with various reaction mechanisms in the AMAR model were determined by simulating indoor chamber data obtained from controlled experimental conditions (Table 1). The simulation of chamber data using the model was performed using a kinetic solver (Morpho) (Jeffries, 1998). In these mechanisms, the symbols “g”, “aq”, and “d” denote the chemical species in the gas phase, inorganic–salt seeded aqueous phase, and dust phase, respectively. The unit of concentration of chemical species is molecule per cm^3 of air. In the following sections, the components of the AMAR model are described in detail.

3.1 SO₂ oxidation in gas phase and aerosol aqueous phase

3.1.1 Gas phase oxidation

The oxidation of SO₂ in the gas phase has been extensively studied by numerous researchers (Baulch et al., 1984; Kerr, 1984; Atkinson and Lloyd, 1984; Calvert, 1984; Graedel, 1977; Atkinson et al., 1989). In this study, the oxidation of SO₂ is described using comprehensive reaction mechanisms shown in Table S1. The mechanisms can also be simplified as follows:



3.1.2 Gas–aerosol partitioning

SO₂ is dissolved into hygroscopic sulfuric acid (H₂SO₄), which is formed in the gas phase, *via* a partitioning process and reacts with the aqueous phase oxidants (e.g. H₂O₂ and O₃) to heterogeneously form H₂SO₄. The chemical species that were treated by the partitioning process include SO₂, NO_x, O₃, OH, HO₂, H₂O₂, HCOOH, CH₃OOH, HNO₃, CH₃O₂, HONO, CH₃COOH, and HCHO. In the model, the partitioning process is approached using the gas–particle partitioning coefficient K_{aq,SO_2} ($\text{m}^3 \mu\text{g}^{-1}$) based on aerosol mass concentration. K_{aq,SO_2} is derived from Henry’s law constant of SO₂ ($K_{H,\text{SO}_2}=1.2K_H$, mol L⁻¹ atm⁻¹ at 298K) (Chameides, 1984),

$$K_{aq,SO_2} = \frac{K_{H,SO_2}RT}{\rho_{aq}} \quad (1)$$

where R is the ideal gas constant ($J K^{-1} mol^{-1}$) and ρ_{aq} ($g cm^{-3}$) is the density of the particle, which is calculated using inorganic thermodynamic model (E-AIM II) (Clegg et al., 1998; Wexler and Clegg, 2002; Clegg and Wexler, 2011) based on humidity and inorganic composition. The

5 absorption-desorption process of SO_2 on inorganic aerosol (In_{aq}) is expressed as,



$k_{abs,SO_2,aq}$ ($s^{-1} m^3 m^{-2}$) and $k_{des,SO_2,aq}$ (s^{-1}) are the absorption rate constant and the desorption rate constant, respectively, and are calculated as follows,

$$10 \quad k_{abs,SO_2,aq} = f_{abs,aq} \frac{\omega_{SO_2} f_{aq,M2S}}{4} \quad (2)$$

$$k_{des,SO_2,aq} = \frac{k_{abs,SO_2,aq}}{K_{aq}} \quad (3)$$

where $f_{aq,M2S}$ (5×10^{-4}) is the coefficient to convert the aerosol mass concentration ($\mu g m^{-3}$) to the surface area concentration ($m^2 m^{-3}$) for particle size near 100 nm and $f_{abs,aq}$ is the coefficient for absorption process. ω_{SO_2} is the mean molecular velocity ($m s^{-1}$) of SO_2 and can be calculated

15 as follows,

$$\omega_{SO_2} = \sqrt{\frac{8RT}{\pi MW}} \quad (4)$$

where MW is molecular weight ($kg mol^{-1}$). ~~In general, the characteristic time (s) of a partitioning process ranges from 10^{-4} s to 10^{-2} s (Freiberg and Schwartz, 1981) and is much faster than both gas phase reaction and the aerosol phase reaction. In our model, $f_{abs,aq}$ was set at 2×10^4 in Eq. (2) to have fast partitioning process. The estimated characteristic time of absorption is 10^{-3} s. In our model, $f_{abs,aq}$ was set at 2×10^4 in Eq. (2) to have fast partitioning process. Table S2 summarizes the characteristic time that is estimated for diffusion, partitioning, and the reactions of major species with OH radicals in gas, aqueous, and dust phases. In general, the characteristic time (s) of a partitioning process (order of 10^{-7} s) is much faster than gas phase oxidation (order of 10^6 s), aqueous phase oxidation (order of 10^3 – 10^4 s), and dust phase oxidation (order of 10^2 – 10^3 s at presence of $200 \mu g m^{-3}$ of dust particles).~~ The mass concentration ($\mu g m^{-3}$) of inorganic seeded aqueous phase above the efflorescent relative humidity (ERH) is also dynamically calculated for the SO_4^{2-} – NH_4^+ – H_2O system. Colberg et al. (2003) semiempirically predicted ERH by fitting to

the experimental data based on the ammonia-to-sulfate ratio in the $\text{SO}_4^{2-}\text{--NH}_4^+\text{--H}_2\text{O}$ system. AMAR model utilizes these parameterizations to predict ERH dynamically. Ammonia is inevitable in our chamber study and mainly acts as a carryover for sulfate from previous chamber experiments. Thus, H_2SO_4 is fully or partially neutralized by ammonia.

5 3.1.3 Aerosol aqueous phase reaction

The AMAR model implements the aqueous-phase chemistry that occurs in inorganic salted aqueous aerosol ($\text{SO}_4^{2-}\text{--NH}_4^+\text{--H}_2\text{O}$ system without ~~no~~ dust) to form $\text{SO}_4^{2-}(\text{aq})$ and $\text{NO}_3^-(\text{aq})$. We employed the preexisting aqueous-phase kinetic reactions involving SO_2 (Liang and Jacobson, 1999) and NO_x chemistry (Liang and Jacobson, 1999; Hoyle et al., 2016). Thus, our simulation inherits all the possible uncertainties embedded in the original kinetic data.

The SO_2 dissolved in the aqueous phase is hydrolyzed into H_2SO_3 and dissociates to form ionic species (HSO_3^- and SO_3^{2-}). $\text{SO}_4^{2-}(\text{aq})$ is formed by reactions of the sulfur species in oxidation state IV (S(IV)(aq)) with $\text{OH}(\text{aq})$, $\text{H}_2\text{O}_2(\text{aq})$, or $\text{O}_3(\text{aq})$ (Table S1). The dissolved HONO can also dissociate to form $\text{NO}_2^-(\text{aq})$ and result to $\text{NO}_3^-(\text{aq})$. Each chemical species in S(IV)(aq) has a different reactivity for oxidation reactions. The distribution of chemical species is affected by aerosol acidity, which is controlled by humidity and inorganic composition. Hence, the formation of sulfate is very sensitive to aerosol acidity. For example, most of the S(IV) is consumed by H_2O_2 at $\text{pH} < 4$, whereas most of it is consumed by O_3 at $\text{pH} > 4$. Some strong inorganic acids, such as sulfuric acid, influence aerosol acidity. In AMAR, aerosol acidity ($[\text{H}^+]$, mol L^{-1}) is predicted using the inorganic thermodynamic model E-AIM II (Clegg et al., 1998; Wexler and Clegg, 2002; Clegg and Wexler, 2011) based on the ammonia-to-sulfate ratio and RH. When the ammonia-to-sulfate ratio is greater than 0.8, the prediction of $[\text{H}^+]$ is corrected based on the method of Li and Jang (2012). At high NO_x levels, $\text{NO}_2^-(\text{aq})$ competes with S(IV)(aq) for the reaction with $\text{OH}(\text{aq})$, O_3 , or H_2O_2 (Table S1) (Ma et al., 2008). However, the HONO concentration becomes high at high NO_x levels and enhances SO_2 oxidation in the inorganic-salt seeded aqueous phase due to the formation of OH radicals *via* photolysis of HONO.

3.2 Heterogeneous oxidation in the presence of mineral dust particles

The heterogeneous chemistry in the presence of dust particles has been newly established in the AMAR model. The dust phase module consists of a partitioning process (Sect. 3.2.1) and

heterogeneous chemistry for SO₂ and other trace gases (ozone, HONO, and NO₂) (Table 3) (Fig. 1). The heterogeneous chemistry of SO₂ is handled by autoxidation (Sect. 3.2.2) and photooxidation under UV light (Sect. 3.2.4). In dust-phase photochemistry, the central mechanism for SO₂ oxidation is operated by the surface oxidants (e.g. OH(d)), which is generated *via* the photoactivation process of semiconductive metal oxides in dust particles (Sect. 3.2.3).

3.2.1 Gas–dust particle partitioning

In an adsorptive mode, water molecules suppress partitioning of SO₂ because they compete for adsorptive sites with tracers (Cwiertny et al., 2008). However, the formation of the sulfate associated with ATD increased as increasing RH as shown in Table 1, suggesting that gas-dust partitioning is more likely operated by an absorption process. ATD contains hygroscopic inorganic salts that form the thin water film on the surface of ATD particles when the salts are deliquescent (or above ERH). This water layer influences the gas-dust partitioning of atmospheric tracers such as SO₂ and NO₂. The gas–dust partitioning constant (K_{d,SO_2} , m³ m⁻²) of SO₂ is defined as,

$$K_{d,SO_2} = \frac{[SO_2]_d}{[SO_2]_g A_{Dust}} \quad (m^3 \text{ m}^{-2}) \quad (5)$$

A_{dust} (m² m⁻³) is the geometric surface concentration of ATD dust particles and is calculated by multiplying the dust mass concentration (μg m³) by a geometric surface–mass ratio ($f_{dust,M2S}$) of ATD particles (3.066×10⁻⁶, m² μg⁻¹). The SO₂ absorption and desorption processes for the dust phase are expressed as



$k_{abs_SO_2,dust}$ (s⁻¹ m³ m⁻²) and $k_{des_SO_2,dust}$ (s⁻¹) are the absorption rate constant and the desorption rate constant, respectively. At equilibrium, the absorption rate (R7) equals the desorption rate (R8). Thus, K_{d,SO_2} can be expressed as

$$K_{d,SO_2} = \frac{k_{abs_SO_2,dust}}{k_{des_SO_2,dust}} \quad (m^3 \text{ m}^{-2}) \quad (6)$$

K_{d,SO_2} is set at 1.63 (m³ m⁻², at 298K for dry particles) based on the literature data (Adams et al., 2005;Huang et al., 2015). The characteristic time to reach to equilibrium is very short (Sect. 3.1.1). In kinetic mechanisms, $k_{abs_SO_2,dust}$ was set at $1.7 \times 10^3 \text{ s}^{-1} \text{ m}^3 \text{ m}^{-2}$ for dry particles (20% RH)

using the same approach as Eq. (2). The resulting characteristic time for $k_{abs,SO_2,dust}$ is 10^{-6} s. The characteristic time of the reaction of SO_2 with an OH radical (10^6 molecules cm^{-3}) is about 10^6 – 10^7 s in gas phase and 10^5 – 10^6 s in both aqueous phase and dust phase.

To consider the effect of temperature on K_{d,SO_2} , the temperature dependency of $k_{des,SO_2,dust}$ (Eq. (6)) is derived from the Henry's constant (Chameides, 1984). K_{d,SO_2} (Eq. (5)) is also influenced by aerosol water content (Zuend et al., 2011) as well as the dissociation of H_2SO_3 , which is operated by aerosol acidity ($[H^+]$) and an acid dissociation constant (Ka_{SO_2}) (Martell and Smith, 1976). Thus, $k_{des,SO_2,dust}$ is expressed as,

$$k_{des,SO_2,dust} = 2 \times 10^9 \exp\left(-\frac{3100}{T}\right) / (F_{water}(1 + \frac{Ka_{SO_2}}{[H^+]}) \text{ (s}^{-1}) \quad (7)$$

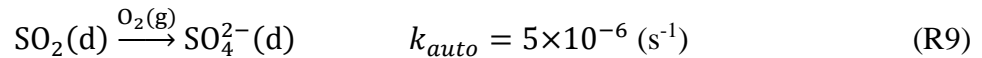
Ka_{SO_2} is 0.013 (mol L^{-1}) at 298K (Martell and Smith, 1976). The influence of the dissociation of inorganic acid on K_{d,SO_2} is accounted for by the term $(1 + \frac{Ka_{SO_2}}{[H^+]})$ in Eq. (7). The estimation of $[H^+]$ is treated in the same ways as aqueous chemistry (Sect. 3.1.3). F_{water} , a numeric number, was introduced into the model to estimate the water fraction of total dust particles. The hygroscopic property of mineral dust dynamically changes because dust can be substantially modified by direct reaction of some of its components (e.g. $CaCO_3$) with inorganic acids such as H_2SO_4 and HNO_3 . When dust forms $Ca(NO_3)_2$, dust becomes more hygroscopic. Nitrate salts deliquesce at very low RH (17%) (Krueger et al., 2003; Krueger et al., 2004; William et al., 2005). $CaSO_4$ is, however, relatively hydrophobic. Nitrate salts exist only when sulfate concentrations is very low. F_{water} originated from the hygroscopic property of indigenous dust (first term in Eq. (8)), the inorganic nitrates formed from the reaction of ~~adsorbed~~–absorbed HNO_3 with dust (second term), the inorganic sulfate (SO_4^{2-} – NH_4^+ – H_2O system, third term).

$$F_{water} = \exp(4.4RH) + 3.7\exp(4.4RH) \frac{[NO_3^-(d_salt)]}{[Dust]} + \frac{M_{in,water}}{[Dust]} \quad (8)$$

$M_{in,water}$ is the water concentration ($\mu g \text{ m}^{-3}$) associated with inorganic sulfate and calculated using E–AIM II. Both $[NO_3^-(d_salt)]$ and $M_{in,water}$ are normalized by the mass concentration of ATD particles ($[Dust]$, $\mu g \text{ cm}^{-3}$). F_{water} is first determined using chamber simulation of SO_2 heterogeneous oxidation (first and third terms in Eq. (8)) (D1–D3 in Table 1) under varied RH levels and extended to SO_2 oxidation in the presence of NO_x (~~L6 and L7 in Table 1~~ Exp. 14 April 2017 in Table 2). Among temperature, RH and aerosol acidity, the most influential variable is RH due to the variation of F_{water} (see sensitivity analysis in Sect. 5).

3.2.2 Autoxidation of SO₂ on dust surface

Typically, autoxidation of SO₂ is an oxidation process *via* the reaction of ~~adsorbed~~ absorbed SO₂ (R7 and R8) with an oxygen molecule. In the model, [SO₄²⁻]_{auto} is defined as the sulfate resulted from any oxidation reactions (autoxidation in open air and oxidation with ozone) of SO₂ without UV light (Fig. 1). In autoxidation, the reaction of SO₂(d) with the oxygen molecules is treated as the first order reaction (assuming the concentration of oxygen is constant as 2 × 10⁵ ppm).



In the dark condition, the formation of sulfate is mainly sourced from ~~The SO₂~~ autoxidation of SO₂. By fitting the predicted concentration of sulfate to the experimental data (D1–D3 in Table 1), the reaction rate constant (k_{auto} , s⁻¹) for SO₂ autoxidation is semiempirically determined ~~by simulating experimental data (D1, D2 and D3 in Table 1)~~. For comparison with other studies, we estimate the reactive uptake coefficient ($\gamma_{\text{SO}_4^{2-}, \text{auto}}$) of SO₂ onto ATD dust in the absence of ozone and NO_x (Fig. 2).

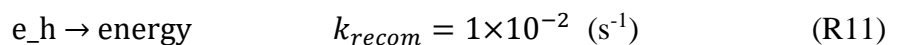
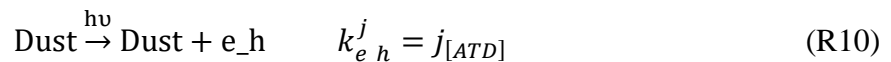
$$\gamma_{\text{SO}_4^{2-}, \text{auto}} = \frac{4K_{d, \text{SO}_2} k_{\text{auto}}}{\omega_{\text{SO}_2}} \quad (9)$$

$\gamma_{\text{SO}_4^{2-}, \text{auto}}$ is proportional to K_{d, SO_2} , and influenced by humidity (Eq. (7)).

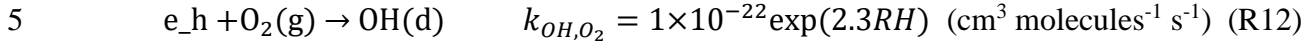
3.2.3 Photoactivation of dust particles and heterogeneous formation of OH radicals

The reactive uptake of SO₂ on particles is traditionally treated as a first order process (Ullerstam et al., 2003; Li et al., 2007). Such an approach is appropriate for simple autoxidation mechanisms, but not for the complex heterogeneous photooxidation of SO₂. In the AMAR model, the heterogeneous photooxidation of SO₂ is approached in three steps: (1) the formation of an e⁻_{cb}–h⁺_{vb} pair *via* photoactivation of dust particles, (2) the formation of OH(d) *via* the reaction of an e⁻_{cb}–h⁺_{vb} pair with a water or oxygen molecule, and (3) the reaction of ~~adsorbed~~ absorbed SO₂ with the resulting OH(d) (second–order reactions) (Table S1).

The photoactivation of dust particles and the recombination reaction of an electron–hole pair (e_{-h}) are added into the model.



where $k_{e_h}^j$ is the photoactivation rate constant to form $e^-_{cb}-h^+_{vb}$ pairs and k_{recom} is the reaction rate constant of recombination (heat radiation) of an electron and a hole. The value of k_{recom} is set at a large number to prevent the accumulation of electron-hole pairs. The formation of OH(d) is expressed as



k_{OH,O_2} is the reaction rate constant to form OH(d) and is first estimated ~~as a function of humidity~~ using indoor chamber data (L2, L3 and L41–L3 in Table 1) at RH 20%, 55% and 80% and then regressed against RH.

In R10, $k_{e_h}^j$ is the operational rate constant for the photoactivation of dust particles and is
 10 dependent on the photolysis rate constant, $j_{[ATD]}$ (s^{-1}). Like the typical photolysis of a gaseous molecule, the photocatalytic production of the $e^-_{cb}-h^+_{vb}$ pair is linear to both the actinic flux ($I(\lambda)$, photons $cm^{-2} nm^{-1} s^{-1}$) originating from the light source and the photocatalytic property of dust particles. The value of $j_{[ATD]}$ is determined by $I(\lambda)$, the absorption cross section ($\sigma(\lambda)$, $cm^2 \mu g^{-1}$), and the quantum yield ($\phi(\lambda)$) of dust conducting matter at each wavelength range (λ , nm),

$$15 \quad j_{[ATD]} = \int_{\lambda_1}^{\lambda_2} I(\lambda) \sigma(\lambda) \phi(\lambda) d\lambda \quad (10)$$

In the model, $\sigma(\lambda)$ is the light absorption needed to activate dust-phase semiconducting metal oxides (excitation from a ground energy level to a conducting band), and $\phi(\lambda)$ is the probability of yielding the $e^-_{cb}-h^+_{vb}$ pair in the dust phase. Both $\sigma(\lambda)$ and $\phi(\lambda)$ cannot be directly measured because of complexity in the quantity of photoactive conducting matter in dust particles and the irradiation
 20 processes of the $e^-_{cb}-h^+_{vb}$ pair. In order to deal with $\sigma(\lambda) \times \phi(\lambda)$, we calculated the mass absorption cross section of dust particles (MAC_{ATD} , $m^2 g^{-1}$), which was determined using the absorption coefficient of ATD particles (b_{ATD} , m^{-1}) with the particle concentration (m_{ATD} , $g m^{-3}$):

$$MAC_{ATD} = \frac{b_{ATD}}{m_{ATD}} \quad (11)$$

In Eq. (11), b_{ATD} can be calculated from the absorbance of dust filter sample (Abs_{ATD} , dimensionless) measured using a reflective UV–visible spectrometer (Fig. S3):
 25

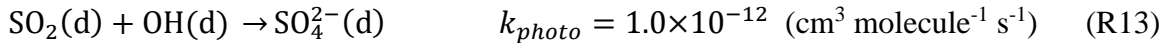
$$b_{ATD} = \frac{Abs_{ATD} A}{f V} \ln(10) \quad (12)$$

where $A = 7.85 \times 10^{-5} (m^2)$ is the sampled area on the filter and $V (m^3)$ is the total air volume passing through the filter during sampling. In order to eliminate the absorbance caused by filter material scattering, a correction factor ($f = 1.4845$) is obtained from a previous study (Zhong and

Jang, 2011) and coupled into Eq. (12). The preliminary study showed that the effect of aerosol scattering on the b_{abs} values of the aerosol collected on the filter was negligible. Further, Bond (2001) reported that particle light scattering does not significantly influence spectral absorption selectivity. The MAC_{ATD} of dust particles originates from photocatalytic conducting matter (e.g. TiO₂) as well as light-absorbing matter (e.g. gypsum and metal sulfate). Thus, the MAC_{ATD} spectrum is adjusted using the known TiO₂ absorption spectrum (Reyes-Coronado et al., 2008) and applied to $\sigma(\lambda) \times \phi(\lambda)$ (Fig. S3). The resulting $\sigma(\lambda) \times \phi(\lambda)$ spectrum is applied to Eq. (10) to calculate $j_{[ATD]}$ (R10).

3.2.4 Heterogeneous photooxidation of SO₂

SO₂ is oxidized by OH(d) on the surface of ATD particles as follows,



where k_{photo} is the reaction rate constant of SO₂ with OH(d) and is estimated from gas phase reaction (R1). Combining Eq. (4), Eq. (5), R11 and R15, the reactive uptake coefficient ($\gamma_{SO_4^{2-},photo}$) of SO₂ on ATD particles under UV light can be written as,

$$\gamma_{SO_4^{2-},photo} = \frac{4K_{d,SO_2}(k_{photo}[OH(d)] + k_{auto})}{\omega_{SO_2}} \quad (13)$$

$\gamma_{SO_4^{2-},photo}$ is the constant at a given concentration of OH(d) (for a given light source, dust concentration, and humidity) (R10 and R12). Figure 2 illustrates $\gamma_{SO_4^{2-},photo}$ values at three different RHs, which were obtained using indoor chamber data. $\gamma_{SO_4^{2-},photo}$ is significantly influenced by both UV light and humidity. For example, $\gamma_{SO_4^{2-},photo}$ is one order of magnitude higher than $\gamma_{SO_4^{2-},auto}$ at low NO_x levels (<5 ppb), and $\gamma_{SO_4^{2-},photo}$ increased from 2.0×10^{-5} to 1.24×10^{-4} when the RH changed from 20% to 80%.

3.3 Impact of ozone and NO_x on heterogeneous chemistry of SO₂

To date, most studies of the effect of NO_x on sulfate formation have been limited to the reaction in dark condition. For example, previous laboratory studies using pure metal oxides reported the acceleration of the heterogeneous oxidation of SO₂ by NO_x in dark conditions (Ma et al., 2008; Liu et al., 2012). For the effect of ozone, the recent chamber study by Park and Jang (2016) showed significant enhancement of heterogeneous photooxidation of SO₂. In the AMAR

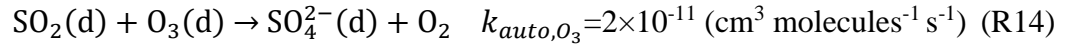
model, the formation of sulfate is also modulated by the involvement of ozone and NO_x in both autoxidation and photochemistry on the surface of dust particles (Fig. 1).

3.3.1 Dust-phase ozone chemistry

- 5 ~~The Like SO₂ (R5 and R6), the~~ gas-dust partitioning coefficient of ozone is scaled using
 K_{d,SO_2} and the ratio of the Henry's law constant of SO₂ (K_{H,SO_2} , Eq. (1)) to that of ozone ($K_{H,O_3} \equiv$
 $1.2 \times 10^{-2} \text{ mol L}^{-1} \text{ atm}^{-1}$ at 298K) (Chameides, 1984), K_{d,O_3} , is determined using the value found
in the literature (Michel et al., 2003; Ullerstam et al., 2002):

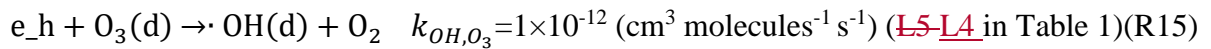
$$K_{d,O_3} = K_{d,SO_2} \frac{K_{H,O_3}}{K_{H,SO_2}} = 7.7 \times 10^{-7} F_{water} = 1.9 \times 10^{-6} \exp\left(\frac{2700}{T}\right) \text{ (m}^3 \text{ m}^{-2}, 20\% \text{ RH)} \quad (14)$$

- 10 The partitioning process is also treated by the adsorption-desorption kinetic mechanism as shown in R7 and R8 (Table 3: partitioning). Ozone can decay catalytically in the dust phase, forming an oxygen molecule and surface-bound atomic oxygen (Usher et al., 2003; Chang et al., 2005). The formed atomic oxygen reacts with SO₂(d) to form sulfate (Ullerstam et al., 2002; Usher et al., 2002):



- 15 k_{auto,O_3} is estimated using indoor chamber data (D4 in Table 1). In the presence of ~~200-300~~ $\mu\text{g m}^{-3}$ of ATD particles and ~~30-60~~ ppb of ozone, the concentration of O₃(d) is estimated as 92.4×10^6 molecule cm⁻³. Under this condition, the characteristic time of the autoxidation by ozone (R14) is 5.2×10^3 s and is much faster than the autoxidation by oxygen (R9, 2×10^5 s). At nighttime, in the presence of ozone, the autoxidation of SO₂(d) yields a significant amount of sulfate.

- 20 Under UV light, ozone is also involved in the production of the surface oxidants (O₃⁻, HO₃ radicals and OH radicals) that further promote heterogeneous oxidation of SO₂. O₃(d) acts as an acceptor for e_{cb}⁻-h_{vb}⁺ and forms OH(d):



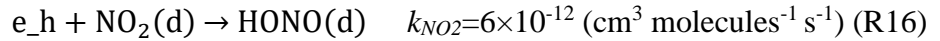
3.3.2 Dust-phase NO_x chemistry

- 25 ~~The gas-dust partitioning coefficient of NO₂ The equilibrium constant of NO₂ on the dust surface~~ (K_{d,NO_2}) is treated as the same approach with ozone, using K_{d,SO_2} and the ratio of K_{H,SO_2}
(Eq. (1)) to the Henry's law constant of NO₂ ($K_{H,NO_2} \equiv 1.2 \times 10^{-2} \text{ mol L}^{-1} \text{ atm}^{-1}$ at 298K)
(Chameides, 1984):

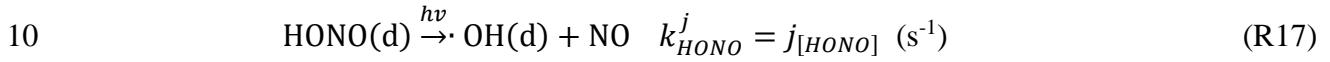
is scaled from K_{d,SO_2} using the known Henry's law constant for SO_2 (K_{H,SO_2} , Eq. (1)) and NO_2 (K_{H,NO_2}) (Chameides, 1984), and written as:

$$K_{d,NO_2} = K_{d,SO_2} \frac{K_{H,NO_2}}{K_{H,SO_2}} = 1.5 \times 10^{-6} F_{water} 3.7 \times 10^{-6} \exp\left(\frac{2500}{T}\right) (\text{m}^3 \text{m}^{-2}, 20\% \text{ RH}) \quad (15)$$

- 5 The ~~adsorbed~~-absorbed NO_2 first reacts with $e_{cb}^-(d)$ or $\cdot O_2^-(d)$ on the dust surface (R10) and forms HONO(d) (Ma et al., 2008; Liu et al., 2012; Saliba and Chamseddine, 2012; Saliba et al., 2014). In AMAR, the formation of HONO(d) is simplified into:

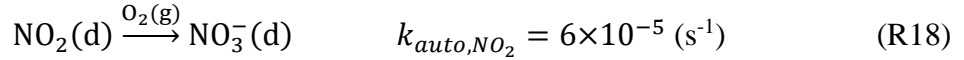


HONO(d) is further decomposed through photolysis and yields OH(d):

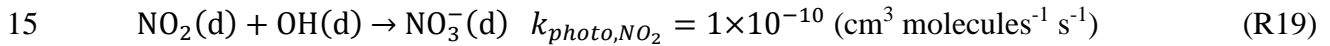


The photolysis rate constant of HONO(d) is treated with the one for gaseous HONO ($j_{[HONO]}$).

Similar to autoxidation of SO_2 (Sect. 3.2.2), $NO_2(d)$ autoxidizes to form nitrate:



NO_2 reacts with OH(d):



k_{auto,NO_2} and k_{photo,NO_2} was determined using the simulation of ~~indoor-outdoor~~ chamber data (L7 and L8 Exp. 14 April 2017 in Table 42). The estimation of the gas-dust partitioning

coefficients of HONO ($K_{d,HONO}$) (Becker et al., 1996) and HNO_3 (K_{d,HNO_3}) (Schwartz and White, 1981) was approached using the similar method for SO_2 (Table 3). N_2O_5 forms nitrate *via* a

- 20 reactive uptake process as shown in Table 3 (reaction 11).

4 Simulation of AMAR model under ambient sunlight

At the beginning of the development of the AMAR model, the kinetic parameters to predict the formation of sulfate and nitrate in the presence of ATD particles were leveraged using an indoor chamber. In order to test the feasibility of the resulting AMAR model, the UF-APHOR data using
25 natural sunlight were simulated (Table 2). The chamber dilution (measured by CCl_4) and the wall process of gaseous compounds (e.g. ozone, SO_2 , HONO, NO_2) and particles were integrated with the kinetic mechanisms to simulate UF-APHOR data (Sect. S1). As shown in Fig. 1, the model inputs are the concentration of chemical species, the amount of dust, and the meteorological

variables that are commonly found at regional scales. The dual chambers allow for two controlled experiments to be performed simultaneously under the same meteorological conditions.

4.1 Simulations for different dust loadings

Figure 3 shows that the predicted $[\text{SO}_4^{2-}]_T$ is in good agreement with experimental observations, which were performed under low NO_x conditions ($\text{NO}_x < 5$ ppb) for two different dust loadings as well as two different SO_2 levels. The greater increase in $[\text{SO}_4^{2-}]_T$ appeared with the higher sunlight intensity (between 11 AM and 2 PM). In Fig. 3(a), the predicted $[\text{SO}_4^{2-}]_T$ increased by 63% (at 3 PM) with $290 \mu\text{g m}^{-3}$ of ATD particles compared to the $[\text{SO}_4^{2-}]_T$ without dust particles. Figure 3(b) confirms that the larger dust particle loading yields more $[\text{SO}_4^{2-}]_T$. In Fig. 3(c), $[\text{SO}_4^{2-}]_T$ was predicted with high and low initial concentrations of SO_2 for a given dust loading. The time profiles of the simulation of concentrations of NO_x , ozone, SO_2 and dust are shown in Fig. S4.

Because of the large size of dust particles, the wall processes (e.g. settling and wall deposition) of dust particles is greater than that of the sulfate particles originated from $[\text{SO}_4^{2-}]_{\text{aq}}$ (no dust). Hence, the fraction of $[\text{SO}_4^{2-}]_{\text{dust}}$ to $[\text{SO}_4^{2-}]_T$ declines over the course of the chamber experiment. To estimate how the predicted $[\text{SO}_4^{2-}]_T$ is attributed to $[\text{SO}_4^{2-}]_{\text{aq}} + [\text{SO}_4^{2-}]_{\text{gas}}$ (non-dust sulfate) and $[\text{SO}_4^{2-}]_{\text{dust}}$ without wall processes, Fig. 3(d), 3(e), and 3(f) are reconstructed from Fig. 3(a), 3(b), and 3(c), respectively. As shown in the inner pie chart of Fig. 3(d), a significant fraction of $[\text{SO}_4^{2-}]_T$ is attributed to dust phase chemistry ($[\text{SO}_4^{2-}]_{\text{auto}} + [\text{SO}_4^{2-}]_{\text{photo}} : 0.58$) ~~$[\text{SO}_4^{2-}]_{\text{dust}} (0.73)$~~ . Only the 0.03 of $[\text{SO}_4^{2-}]_T$ originates from autoxidation. In Fig. 3(e), the fraction of final $[\text{SO}_4^{2-}]_{\text{dust photo}}$ to $[\text{SO}_4^{2-}]_T$ increases from 0.48-0.28 to 0.85-0.72 with the increase of dust loading from $90 \mu\text{g m}^{-3}$ to $403 \mu\text{g m}^{-3}$. The increased dust loading promotes both the adsorption ~~absorption~~ of SO_2 onto dust particles and the production of dust-phase oxidants, and thus yields more sulfate production. With the increase of the initial concentration of SO_2 from 119 ppb to 272 ppb in Fig. 3(f), the fraction of $[\text{SO}_4^{2-}]_{\text{dust photo}}$ fraction and $[\text{SO}_4^{2-}]_{\text{gas}} + [\text{SO}_4^{2-}]_{\text{aq}}$ are not much changed, while decreases from 0.5 to 0.33, although $[\text{SO}_4^{2-}]_T$ increases from 1716.6 $\mu\text{g m}^{-3}$ to 2830.12 $\mu\text{g m}^{-3}$. The elevation of the high-concentration of SO_2 increases-produces more sulfate formation in the gas all three phases (gas, aqueous, and dust phases) and subsequently promotes aqueous phase chemistry. The sulfuric acid formed in the aqueous phase is hydrophilic and creates a positive feedback loop

which aggravates the growth of aqueous aerosol. Overall, the variation in dust concentration is more influential on $[\text{SO}_4^{2-}]_{\text{T-photo}}$ than that of SO_2 .

4.2 Simulation of NO_x effect

Figure 4 shows that the model performs well in predicting $[\text{SO}_4^{2-}]_{\text{T}}$ in various levels of NO_x . ~~Both the model predicted and observed $[\text{SO}_4^{2-}]_{\text{T}}$ are lower at higher NO_x . The concentrations of background hydrocarbon in Fig. 4(a) and Fig. 4(b) are low (no additional hydrocarbons, Sect. S1), while 30 ppb of isoprene were injected in Fig. 4(c) to increase the amount of ozone. Isoprene oxidation in the gas phase was simulated using MCM (version 3.3.1) (Jenkin et al., 1997; Saunders et al., 2003).~~ Figure 4(d) is reconstructed from Fig. 4(a), 4(b) and 4(c) to illustrate how $[\text{SO}_4^{2-}]_{\text{T}}$ is attributed to the aqueous-phase reaction ($[\text{SO}_4^{2-}]_{\text{gas}} + [\text{SO}_4^{2-}]_{\text{aq}}$), dust-phase autoxidation ($[\text{SO}_4^{2-}]_{\text{auto}}$), and dust photochemistry ($[\text{SO}_4^{2-}]_{\text{photo}}$). Comparing Fig. 4(b) with 4(c), $[\text{SO}_4^{2-}]_{\text{photo}}$ is suppressed at high NO_x levels because NO_2 competes for the consumption of dust-phase OH radicals with SO_2 . The reduction of $[\text{SO}_4^{2-}]_{\text{T}}$ in the afternoon is due to the particle loss at the low concentrations of SO_2 . The simulated concentrations of NO_x , ozone, SO_2 and dust are shown in Fig. S5.

The time profiles of the predicted $[\text{NO}_3^-]_{\text{T}}$ are also shown in Fig. 4(a), 4(b), and 4(c). In the morning, NO_2 quickly oxidizes to accumulate nitric acid in the dust phase. The dust-phase nitric acid might rapidly react with alkaline carbonates (e.g. K, Na, Ca and Mg ions) in the dust phase and form nitrate salts ($\text{NO}_3^- (\text{d_salt})$ in reaction 12 in Table 3). As described in Sect. 3.2.1, these nitrate salts are very hygroscopic and further enhance gas-dust partitioning of gaseous species including HNO_3 , SO_2 , and HONO at high humidity (in the morning). With increasing sunlight intensity, the temperature increases but humidity decreases (20%, Fig. S6) and thus increase the desorption of HNO_3 . In addition to meteorological conditions, the formation of low-volatility sulfuric acid can deplete nitrate *via* evaporation of volatile nitric acid ($\text{SO}_4^{2-} (\text{d_salt})$ in reaction 13 and 14 in Table 3) from the dust surface. The capacity of ATD particles to form nitrate salts (or sulfate salts) is limited by the amount of carbonates and metal oxides on the surface of dust particles. This capacity is estimated to be 0.6 ppb (the number concentration of reactive sites in air), which was determined by comparing the actual aerosol acidity, as measured by the colorimetry integrated with a reflectance UV-visible spectrometer (C-RUV), to the aerosol acidity predicted by the inorganic thermodynamic model (E-AIM II) using the inorganic composition

from PILS-IC (Li et al., 2015;Beardsley and Jang, 2016). As shown in Fig. 4, the effect of HNO_3 on the heterogeneous reaction is negligible during daytime because sulfuric acid, a strong acid, depletes partitioning of HNO_3 (Eq. (15)). At the end of the photooxidation, nitrate is slightly underestimated because some observed nitrate may be trapped under the layer of hydrophobic alkaline sulfate formed *via* aging of ATD particles (effloresced). The surface HONO(d) , which formed *via* the photocatalytic process of NO_2 (R16), can influence the production of OH(d) . However, the model analysis originated from the integrated reaction rate (IRR), an accumulated flux of chemical formation, suggests that the contribution of HONO(d) to OH(d) production is relatively small compared to the direct photocatalytic process caused by dust particles shown in Sect. 3.2.3.

5 Sensitivity and uncertainties

The sensitivity of sulfate prediction to major variables (e.g. temperature, humidity, sunlight profile, the concentration of SO_2 and NO_x , and dust loading) is illustrated in Fig. 5. To avoid the suppression of dust chemistry at high NO_x levels, the most sensitivity tests were performed at low levels of NO_x . The stacked chart normalized with $[\text{SO}_4^{2-}]$ in Fig. 5 shows how $[\text{SO}_4^{2-}]_{\text{T}}$ is attributed to $[\text{SO}_4^{2-}]_{\text{auto}}$, $[\text{SO}_4^{2-}]_{\text{photo}}$ and $[\text{SO}_4^{2-}]_{\text{aq}} + [\text{SO}_4^{2-}]_{\text{gas}}$ (non-dust chemistry).

Figure 5(a) illustrates that the reduction of $[\text{SO}_4^{2-}]_{\text{T}}$ at a higher temperature (273K vs. 298K) is ascribed to the decrease in the partitioning process. Figure 5(b) shows that $[\text{SO}_4^{2-}]_{\text{T}}$ increases by a factor of ~~32.5~~ 8 with RH increasing from 25% to 80%. Humidity plays an important role in the modulation of both aerosol acidity and liquid water content, and ultimately influences the partitioning process (e.g. SO_2 partitioning on dust surface) and dust-phase chemistry (e.g. production of OH(d)). In the stacked column chart of Fig. 5(b), the contribution of $[\text{SO}_4^{2-}]_{\text{dust}}$ to $[\text{SO}_4^{2-}]_{\text{T}}$ increases from ~~0.64~~ 73 to ~~0.79~~ 86 with increasing RH suggesting that dust chemistry is more sensitive to humidity than aqueous phase chemistry. Figure 5(c) presents $[\text{SO}_4^{2-}]_{\text{T}}$ at two different sunlight intensities (winter on ~~1222~~ November, 201~~56~~ vs. summer on ~~25 11 May~~ April, 2015 2017) in Gainesville, Florida (latitude/longitude: 29.64185°/-82.347883°). As shown in Fig. 5(d), with SO_2 concentrations increasing from 20 ppb to 100 ppb, $[\text{SO}_4^{2-}]_{\text{T}}$ increases by a factor of ~~two~~ 4.4 in the given simulation condition. The effect of the concentration of SO_2 on $[\text{SO}_4^{2-}]_{\text{T}}$ has been discussed in Sect. 4.1 above. Figure 5(e) shows the sensitivity of $[\text{SO}_4^{2-}]_{\text{T}}$ to the ATD loading (100, 200, and 400 $\mu\text{g m}^{-3}$). With the increasing of dust loading, the contribution of $[\text{SO}_4^{2-}]_{\text{photo}}$ to

$[\text{SO}_4^{2-}]_{\text{T}}$ also increases. Figure 5(f) illustrates how sulfate formation is suppressed by different NO_x levels (also see Sect. 3.3.2).

Figure S7 illustrates the influence of the uncertainties in the major model parameters on the prediction of $[\text{SO}_4^{2-}]_{\text{T}}$. The uncertainty in K_{d, SO_2} ($\pm 16\%$) of SO_2 was determined using a value from the literature (Adams et al., 2005). The variation in $[\text{SO}_4^{2-}]_{\text{T}}$ due to the uncertainty in K_{d, SO_2} is as small as $\pm 2\%$. The reaction rate constants of dust chemistry in the model (Table 3) were semi-empirically determined using preexisting indoor chamber data (Park and Jang, 2016) and chamber characterization. The uncertainty in rate constants associated with observed sulfate concentrations is about $\pm 10\%$. Fig. S7 also shows the variation in $[\text{SO}_4^{2-}]_{\text{T}}$ due to the uncertainty in both the reaction of SO_2 with dust-surface OH radicals (k_{photo}) and the production rate constant of dust-surface OH radicals ($k_{\text{OH}, \text{O}_2}$). Among K_{d, SO_2} , k_{photo} , and $k_{\text{OH}, \text{O}_2}$, the highest uncertainty appears in $k_{\text{OH}, \text{O}_2}$.

Most simulations of sulfate in this study are limited to environmental conditions under low concentrations of hydrocarbons. In the future, the model should be evaluated for the chamber data generated from various mixes of SO_2 , NO_x , and hydrocarbons in the presence of mineral dust. The inorganic thermodynamic model (e.g. E-AIM II) was employed here to estimate $[\text{H}^+]$ and the liquid water content ($M_{\text{in}, \text{water}}$) for the $\text{SO}_4^{2-}\text{--NH}_4^+\text{--H}_2\text{O}$ system (excluding $\text{SO}_4^{2-}(\text{d_salt})$ in reaction 13 of Table 3: dust phase) (Eq. (8)) in both inorganic-salt seeded aqueous phase and dust phase chemistry. The uncertainty in $M_{\text{in}, \text{water}}$ and $[\text{H}^+]$ influences partitioning of SO_2 and NO_x , as well as $[\text{SO}_4^{2-}]_{\text{T}}$. The uncertainties in the prediction of $[\text{H}^+]$ using inorganic thermodynamic models are large because of the limited data (Clegg et al., 1998; Wexler and Clegg, 2002), especially for ammonia-rich inorganic salts in the low RH range. In this study, our model uses the corrected estimation of $[\text{H}^+]$ based on the filter-based C-RUV technique (Li et al., 2015). The estimated uncertainty in the C-RUV method is $\pm 18\%$, and results in a $\pm 7\%$ variation in $[\text{SO}_4^{2-}]_{\text{T}}$. The dust surface area in AMAR is calculated using the geometric surface area. To extend the AMAR model to other dust materials, the molecular level surface area (BET surface area) should be considered in the future.

6 Conclusion and atmospheric implication

The AMAR model of this study was developed to predict the oxidation of SO₂ and NO_x using comprehensive kinetic mechanisms in the gas phase, inorganic seeded aqueous phase, and dust phase. The thermodynamic parameters engaged in the partitioning process between gas, inorganic salted aqueous aerosol and dust phases were obtained from known data in the literature (Table 3), and the kinetic parameters for dust chemistry were estimated using previously reported indoor chamber data (Park and Jang, 2016). Overall, the AMAR simulations were consistent with experimentally observed outdoor chamber data (Fig. 3 and Fig. 4) under ambient sunlight. As discussed in the sensitivity analysis (Sect. 5), both the [SO₄²⁻]_T and the relative distribution of mechanism-based sulfate formation are sensitive to all major variables (model inputs) including temperature, humidity, sunlight intensity, the quantity of dust loading, and concentrations of NO_x and SO₂.

In order to assess the importance of dust chemistry in ambient conditions, the prediction of sulfate formation in the presence of ATD dust needs to be extended to 24 h simulations under various environmental conditions. Figure S8 shows the output simulated for 24 h with 200 µg m⁻³ of ATD particle loading under urban (40 ppb NO_x; VOC/NO_x < 5; 20 ppb SO₂) and rural atmospheres (5 ppb NO_x; VOC/NO_x > 20; 2 ppb SO₂). At nighttime, when the temperature drops and humidity increases (70–90%, Fig. S6), the contribution of [SO₄²⁻]_{auto} to [SO₄²⁻]_T becomes larger than the typical chamber simulation during the daytime. In a rural environment, [SO₄²⁻]_{photo} is still the most influential on sulfate formation (0.57–76 fraction of [SO₄²⁻]_T in Fig. S8(a)). For the simulation in a polluted area (Fig. S8(b)), the fraction of [SO₄²⁻]_{photo} to [SO₄²⁻]_T significantly decreases (0.61–43) because of the suppression induced by NO_x (Sect. 3.3.2), but the fraction of [SO₄²⁻]_{auto} to [SO₄²⁻]_T increases (0.34–28). With decreasing sunlight intensity (after 5 PM), Fig. S8 shows the rapid increases in [SO₄²⁻]_{auto} due to the reaction of dust-phase SO₂ with ozone, which is the result of daytime photooxidation (Sect. 3.3.1). Fig. S8 suggests that the failure to predict sulfate formation without accurate dust chemistry ([SO₄²⁻]_{auto} + [SO₄²⁻]_{photo}) can lead to substantial underestimation of the quantity of total sulfate at regional or global scales. SO₂ autooxidation alone may partially improve the prediction of sulfate in the presence of mineral dust, but sulfate production can still be largely underestimated and incorrectly predicted in time series when heterogeneous photocatalytic reactions in kinetic mechanisms are not considered.

The ATD particles in this study have chemical and physical properties different from ambient mineral dust particles. In general, the uptake coefficient of SO₂ in authentic mineral dust particles (e.g. Gobi Desert dust and Saharan dust) is known to be higher than that of ATD particles (Crowley et al., 2010). Thus, the effect of ambient dust particles on heterogeneous photocatalytic oxidation would be much more important than that of the ATD particles of this study. To extend the AMAR model to the prediction of sulfate in the presence of ambient dust particles, the model parameters related to rate constants, partitioning process, and the physical characteristics (e.g. surface area) of dust particles need to be updated with chamber data.

Acknowledgments

- 10 This work was supported by grants from the National Institute of Metrological Science (NIMS–2016–3100), the Ministry of Science, ICT, and Future Planning at South Korea (2014M3C8A5032316) and the Fulbright Scholar (from USA to Mongolia).

References

- Adams, J. W., Rodriguez, D., and Cox, R. A.: The uptake of SO₂ on Saharan dust: a flow tube study, *Atmos Chem Phys*, 5, 2679-2689, 2005.
- Atkinson, R., Baulch, D., Cox, R., Hampson Jr, R., Kerr, J., Rossi, M., and Troe, J.: Evaluated kinetic and photochemical data for atmospheric chemistry: supplement VI. IUPAC subcommittee on gas kinetic data evaluation for atmospheric chemistry, *Journal of Physical and Chemical Reference Data*, 26, 1329-1499, 1997.
- Beardsley, R. L., and Jang, M.: Simulating the SOA formation of isoprene from partitioning and aerosol phase reactions in the presence of inorganics, *Atmos Chem Phys*, 16, 5993-6009, 2016.
- Becker, K. H., Kleffmann, J., Kurtenbach, R., and Wiesen, P.: Solubility of nitrous acid (HONO) in sulfuric acid solutions, *The Journal of Physical Chemistry*, 100, 14984-14990, 1996.
- Binkowski, F. S., and Roselle, S. J.: Models-3 Community Multiscale Air Quality (CMAQ) model aerosol component 1. Model description, *Journal of geophysical research: Atmospheres*, 108, 2003.
- Bond, T. C.: Spectral dependence of visible light absorption by carbonaceous particles emitted from coal combustion, *Geophys Res Lett*, 28, 4075-4078, Doi 10.1029/2001gl013652, 2001.
- Bongartz, A., Kames, J., Welter, F., and Schurath, U.: Near-UV absorption cross sections and trans/cis equilibrium of nitrous acid, *The Journal of Physical Chemistry*, 95, 1076-1082, 1991.
- Byun, D., and Schere, K. L.: Review of the governing equations, computational algorithms, and other components of the models-3 Community Multiscale Air Quality (CMAQ) modeling system, *Appl Mech Rev*, 59, 51-77, 10.1115/1.2128636, 2006.
- Chameides, W. L.: The photochemistry of a remote marine stratiform cloud, *Journal of Geophysical Research: Atmospheres*, 89, 4739-4755, 1984.
- Chang, R. Y. W., Sullivan, R. C., and Abbatt, J. P. D.: Initial uptake of ozone on Saharan dust at atmospheric relative humidities, *Geophys Res Lett*, 32, Artn L14815 10.1029/2005gl023317, 2005.
- Chen, H. H., Nanayakkara, C. E., and Grassian, V. H.: Titanium Dioxide Photocatalysis in Atmospheric Chemistry, *Chem Rev*, 112, 5919-5948, 10.1021/cr3002092, 2012.
- Clegg, S., and Wexler, A. S.: Densities and Apparent Molar Volumes of Atmospherically Important Electrolyte Solutions. 2. The Systems H⁺-HSO₄⁻-SO₄²⁻-H₂O from 0 to 3 mol kg⁻¹ as a Function of Temperature and H⁺-NH₄⁺-HSO₄⁻-SO₄²⁻-H₂O from 0 to 6 mol kg⁻¹ at 25° C Using a Pitzer Ion Interaction Model, and NH₄HSO₄-H₂O and (NH₄)₃H(SO₄)₂-H₂O over the Entire Concentration Range, *The Journal of Physical Chemistry A*, 115, 3461-3474, 2011.
- Clegg, S. L., Brimblecombe, P., and Wexler, A. S.: Thermodynamic model of the system H⁺-NH₄⁺-SO₄²⁻-NO₃⁻-H₂O at tropospheric temperatures, *The Journal of Physical Chemistry A*, 102, 2137-2154, 1998.
- Colberg, C., Luo, B., Wernli, H., Koop, T., and Peter, T.: A novel model to predict the physical state of atmospheric H₂SO₄/NH₃/H₂O aerosol particles, *Atmos Chem Phys*, 3, 909-924, 2003.
- Colmenares, J. C., and Luque, R.: Heterogeneous photocatalytic nanomaterials: prospects and challenges in selective transformations of biomass-derived compounds, *Chem Soc Rev*, 43, 765-778, 10.1039/c3cs60262a, 2014.

- Crowley, J. N., Ammann, M., Cox, R. A., Hynes, R. G., Jenkin, M. E., Mellouki, A., Rossi, M. J., Troe, J., and Wallington, T. J.: Evaluated kinetic and photochemical data for atmospheric chemistry: Volume V - heterogeneous reactions on solid substrates, *Atmos Chem Phys*, 10, 9059-9223, 10.5194/acp-10-9059-2010, 2010.
- 5 Cwiertny, D. M., Young, M. A., and Grassian, V. H.: Chemistry and photochemistry of mineral dust aerosol, *Annu Rev Phys Chem*, 59, 27-51, 10.1146/annurev.physchem.59.032607.093630, 2008.
- Dong, X., Fu, J. S., Huang, K., Tong, D., and Zhuang, G.: Model development of dust emission and heterogeneous chemistry within the Community Multiscale Air Quality modeling
10 system and its application over East Asia, *Atmos. Chem. Phys.*, 16, 8157-8180, 10.5194/acp-16-8157-2016, 2016.
- Dupart, Y., King, S. M., Nekat, B., Nowak, A., Wiedensohler, A., Herrmann, H., David, G., Thomas, B., Miffre, A., Rairoux, P., D'Anna, B., and George, C.: Mineral dust photochemistry induces nucleation events in the presence of SO₂, *P Natl Acad Sci USA*,
15 109, 20842-20847, 10.1073/pnas.1212297109, 2012.
- Dupart, Y., Fine, L., D'Anna, B., and George, C.: Heterogeneous uptake of NO₂ on Arizona Test Dust under UV-A irradiation: An aerosol flow tube study, *Aeolian Res*, 15, 45-51, 10.1016/j.aeolia.2013.10.001, 2014.
- Gankanda, A., Coddens, E. M., Zhang, Y., Cwiertny, D. M., and Grassian, V. H.: Sulfate
20 formation catalyzed by coal fly ash, mineral dust and iron (iii) oxide: variable influence of temperature and light, *Environmental Science: Processes & Impacts*, 18, 1484-1491, 2016.
- Goodman, A. L., Li, P., Usher, C. R., and Grassian, V. H.: Heterogeneous uptake of sulfur dioxide on aluminum and magnesium oxide particles, *J Phys Chem A*, 105, 6109-6120, 10.1021/jp004423z, 2001.
- 25 Hoffmann, M. R., Martin, S. T., Choi, W. Y., and Bahnemann, D. W.: Environmental Applications of Semiconductor Photocatalysis, *Chem Rev*, 95, 69-96, DOI 10.1021/cr00033a004, 1995.
- Hoyle, C. R., Fuchs, C., Jarvinen, E., Saathoff, H., Dias, A., El Haddad, I., Gysel, M., Coburn, S. C., Trostl, J., Bernhammer, A. K., Bianchi, F., Breitenlechner, M., Corbin, J. C., Craven, J.,
30 Donahue, N. M., Duplissy, J., Ehrhart, S., Frege, C., Gordon, H., Hoppel, N., Heinritzi, M., Kristensen, T. B., Molteni, U., Nichman, L., Pinterich, T., Prevot, A. S. H., Simon, M., Slowik, J. G., Steiner, G., Tome, A., Vogel, A. L., Volkamer, R., Wagner, A. C., Wagner, R., Wexler, A. S., Williamson, C., Winkler, P. M., Yan, C., Amorim, A., Dommen, J., Curtius, J., Gallagher, M. W., Flagan, R. C., Hansel, A., Kirkby, J., Kulmala, M., Mohler,
35 O., Stratmann, F., Worsnop, D. R., and Baltensperger, U.: Aqueous phase oxidation of sulphur dioxide by ozone in cloud droplets, *Atmos Chem Phys*, 16, 1693-1712, 10.5194/acp-16-1693-2016, 2016.
- Huang, L. B., Zhao, Y., Li, H., and Chen, Z. M.: Kinetics of Heterogeneous Reaction of Sulfur Dioxide on Authentic Mineral Dust: Effects of Relative Humidity and Hydrogen Peroxide,
40 *Environ Sci Technol*, 49, 10797-10805, 10.1021/acs.est.5b03930, 2015.
- Krueger, B. J., Grassian, V. H., Laskin, A., and Cowin, J. P.: The transformation of solid atmospheric particles into liquid droplets through heterogeneous chemistry: Laboratory insights into the processing of calcium containing mineral dust aerosol in the troposphere, *Geophys Res Lett*, 30, Artid 1148
45 10.1029/2002gl016563, 2003.

- Li, J., Jang, M., and Beardsley, R. L.: Dialkylsulfate formation in sulfuric acid-seeded secondary organic aerosol produced using an outdoor chamber under natural sunlight, *Environ Chem*, 2015.
- Li, J. W., and Han, Z. W.: A modeling study of the impact of heterogeneous reactions on mineral aerosol surfaces on tropospheric chemistry over East Asia, *Particuology*, 8, 433-441, 10.1016/j.partic.2010.03.018, 2010.
- Liang, J. Y., and Jacobson, M. Z.: A study of sulfur dioxide oxidation pathways over a range of liquid water contents, pH values, and temperatures, *J Geophys Res-Atmos*, 104, 13749-13769, Doi 10.1029/1999jd900097, 1999.
- Linsebigler, A. L., Lu, G. Q., and Yates, J. T.: Photocatalysis on TiO_2 Surfaces - Principles, Mechanisms, and Selected Results, *Chem Rev*, 95, 735-758, DOI 10.1021/cr00035a013, 1995.
- Liu, C., Ma, Q. X., Liu, Y. C., Ma, J. Z., and He, H.: Synergistic reaction between SO_2 and NO_2 on mineral oxides: a potential formation pathway of sulfate aerosol, *Phys Chem Chem Phys*, 14, 1668-1676, 10.1039/c1cp22217a, 2012.
- Liu, Y., Zhu, T., Zhao, D., and Zhang, Z.: Investigation of the hygroscopic properties of $\text{Ca}(\text{NO}_3)_2$ and internally mixed $\text{Ca}(\text{NO}_3)_2/\text{CaCO}_3$ particles by micro-Raman spectrometry, *Atmos Chem Phys*, 8, 7205-7215, 2008.
- Ma, Q. X., Liu, Y. C., and He, H.: Synergistic effect between NO_2 and SO_2 in their adsorption and reaction on gamma-alumina, *J Phys Chem A*, 112, 6630-6635, 10.1021/jp802025z, 2008.
- Martell, A. E., and Smith, R. M.: *Inorganic complexes*, Plenum Press, 1976.
- McNaught, A. D., and Wilkinson, A.: *IUPAC. Compendium of Chemical Terminology*, 2nd ed. (the "Gold Book"), WileyBlackwell; 2nd Revised edition edition, 1997.
- Michel, A. E., Usher, C. R., and Grassian, V. H.: Reactive uptake of ozone on mineral oxides and mineral dusts, *Atmos Environ*, 37, 3201-3211, 10.1016/S1352-2310(03)00319-4, 2003.
- Nanayakkara, C. E., Pettibone, J., and Grassian, V. H.: Sulfur dioxide adsorption and photooxidation on isotopically-labeled titanium dioxide nanoparticle surfaces: roles of surface hydroxyl groups and adsorbed water in the formation and stability of adsorbed sulfite and sulfate, *Phys Chem Chem Phys*, 14, 6957-6966, 10.1039/c2cp23684b, 2012.
- Navea, J. G., Chen, H. H., Huang, M., Carmichel, G. R., and Grassian, V. H.: A comparative evaluation of water uptake on several mineral dust sources, *Environ Chem*, 7, 162-170, 10.1071/En09122, 2010.
- Park, J., and Jang, M.: Heterogeneous photooxidation of sulfur dioxide in the presence of airborne mineral dust particles, *RSC Advances*, 6, 58617-58627, 2016.
- Reyes-Coronado, D., Rodríguez-Gattorno, G., Espinosa-Pesqueira, M., Cab, C., De Coss, R., and Oskam, G.: Phase-pure TiO_2 nanoparticles: anatase, brookite and rutile, *Nanotechnology*, 19, 145605, 2008.
- Saliba, N., Moussa, S., and El Tayyar, G.: Contribution of airborne dust particles to HONO sources, *Atmospheric Chemistry and Physics Discussions*, 14, 4827-4839, 2014.
- Saliba, N. A., and Chamseddine, A.: Uptake of acid pollutants by mineral dust and their effect on aerosol solubility, *Atmos Environ*, 46, 256-263, 10.1016/j.atmosenv.2011.09.074, 2012.
- Sarwar, G., Fahey, K., Kwok, R., Gilliam, R. C., Roselle, S. J., Mathur, R., Xue, J., Yu, J., and Carter, W. P.: Potential impacts of two SO_2 oxidation pathways on regional sulfate concentrations: aqueous-phase oxidation by NO_2 and gas-phase oxidation by Stabilized Criegee Intermediates, *Atmos Environ*, 68, 186-197, 2013.

- Sarwar, G., Simon, H., Fahey, K., Mathur, R., Goliff, W. S., and Stockwell, W. R.: Impact of sulfur dioxide oxidation by Stabilized Criegee Intermediate on sulfate, *Atmos Environ*, 85, 204-214, 2014.
- Schwartz, S., and White, W.: Solubility equilibria of the nitrogen oxides and oxyacids in dilute aqueous solution, *Adv. Environ. Sci. Eng.*;(United States), 4, 1981.
- 5 Schwartz, S. E.: Gas-Phase and Aqueous-Phase Chemistry of HO₂ in Liquid Water Clouds, *J Geophys Res-Atmos*, 89, 1589-1598, DOI 10.1029/JD089iD07p11589, 1984.
- Shang, J., Li, J., and Zhu, T.: Heterogeneous reaction of SO₂ on TiO₂ particles, *Sci China Chem*, 53, 2637-2643, 10.1007/s11426-010-4160-3, 2010.
- 10 Tang, M. J., Cziczo, D. J., and Grassian, V. H.: Interactions of Water with Mineral Dust Aerosol: Water Adsorption, Hygroscopicity, Cloud Condensation, and Ice Nucleation, *Chem Rev*, 116, 4205-4259, 10.1021/acs.chemrev.5b00529, 2016.
- Tang, Y. H., Carmichael, G. R., Kurata, G., Uno, I., Weber, R. J., Song, C. H., Guttikunda, S. K., Woo, J. H., Streets, D. G., Wei, C., Clarke, A. D., Huebert, B., and Anderson, T. L.: Impacts of dust on regional tropospheric chemistry during the ACE-Asia experiment: A model study with observations, *J Geophys Res-Atmos*, 109, Artn D19s21 10.1029/2003jd003806, 2004.
- 15 Thompson, T. L., and Yates, J. T.: Surface science studies of the photoactivation of TiO₂ new photochemical processes, *Chem Rev*, 106, 4428-4453, 2006.
- 20 Ullerstam, M., Vogt, R., Langer, S., and Ljungstrom, E.: The kinetics and mechanism of SO₂ oxidation by O₃ on mineral dust, *Phys Chem Chem Phys*, 4, 4694-4699, 10.1039/b203529b, 2002.
- Underwood, G. M., Song, C. H., Phadnis, M., Carmichael, G. R., and Grassian, V. H.: Heterogeneous reactions of NO₂ and HNO₃ on oxides and mineral dust: A combined laboratory and modeling study, *J Geophys Res-Atmos*, 106, 18055-18066, Doi 10.1029/2000jd900552, 2001.
- 25 Usher, C. R., Al-Hosney, H., Carlos-Cuellar, S., and Grassian, V. H.: A laboratory study of the heterogeneous uptake and oxidation of sulfur dioxide on mineral dust particles, *J Geophys Res-Atmos*, 107, Artn 4713 10.1029/2002jd002051, 2002.
- 30 Usher, C. R., Michel, A. E., Stec, D., and Grassian, V. H.: Laboratory studies of ozone uptake on processed mineral dust, *Atmos Environ*, 37, 5337-5347, 10.1016/j.atmosenv.2003.09.014, 2003.
- Vlasenko, A., Sjogren, S., Weingartner, E., Stemmler, K., Gaggeler, H. W., and Ammann, M.: Effect of humidity on nitric acid uptake to mineral dust aerosol particles, *Atmos Chem Phys*, 6, 2147-2160, 2006.
- 35 Wagner, C., Schuster, G., and Crowley, J.: An aerosol flow tube study of the interaction of N₂O₅ with calcite, Arizona dust and quartz, *Atmos Environ*, 43, 5001-5008, 2009.
- Wagner, R., Ajtai, T., Kandler, K., Lieke, K., Linke, C., Muller, T., Schnaiter, M., and Vragel, M.: Complex refractive indices of Saharan dust samples at visible and near UV wavelengths: a laboratory study, *Atmos Chem Phys*, 12, 2491-2512, 10.5194/acp-12-2491-2012, 2012.
- 40 Wexler, A. S., and Clegg, S. L.: Atmospheric aerosol models for systems including the ions H⁺, NH₄⁺, Na⁺, SO₄²⁻, NO₃⁻, Cl⁻, Br⁻, and H₂O, *Journal of Geophysical Research: Atmospheres*, 107, 2002.
- 45

Zhang, X. Y., Zhuang, G. S., Chen, J. M., Wang, Y., Wang, X., An, Z. S., and Zhang, P.: Heterogeneous reactions of sulfur dioxide on typical mineral particles, *J Phys Chem B*, 110, 12588-12596, 10.1021/jp0617773, 2006.

- 5 Zhang, Y.-H., and Chan, C. K.: Understanding the hygroscopic properties of supersaturated droplets of metal and ammonium sulfate solutions using Raman spectroscopy, *The Journal of Physical Chemistry A*, 106, 285-292, 2002.

Zhong, M., and Jang, M.: Light absorption coefficient measurement of SOA using a UV-Visible spectrometer connected with an integrating sphere, *Atmos Environ*, 45, 4263-4271, 10.1016/j.atmosenv.2011.04.082, 2011.

- 10 Zuend, A., Marcolli, C., Booth, A., Lienhard, D., Soonsin, V., Krieger, U., Topping, D., McFiggans, G., Peter, T., and Seinfeld, J.: New and extended parameterization of the thermodynamic model AIOMFAC: calculation of activity coefficients for organic-inorganic mixtures containing carboxyl, hydroxyl, carbonyl, ether, ester, alkenyl, alkyl, and aromatic functional groups, *Atmos Chem Phys*, 11, 9155-9206, 2011.

15

Table 1. Experiment conditions and simulation results for SO₂ heterogeneous photooxidation on the surface of ATD particles at variety condition of humidity (RH), light sources and initial concentration of traces using indoor chamber data.

Exp. No. ^a	UV	RH ^b (%)	Temp. ^b (K)	Initial Concentration				Duration ^e (min)	Exp. [SO ₄ ²⁻] _T ^f (μg m ⁻³)
				ATD dust ^c (μg m ⁻³)	SO ₂ ^d (ppb)	NO/NO ₂ ^d (ppb)	O ₃ ^d (ppb)		
D1	Off	21.0	295.9	295	267	N.A.	N.A.	150	0.61±0.02
D2	Off	55.3	295.0	406	152	0.1/0.6	1.86	148	1.02±0.01
D3	Off	80.1	294.5	278	147	0.9/1.6	0.29	147	1.59±0.02
L1A	On	19.3	296.3	N.A.	92.2	0.4/1.5	0.36	120	1.66±0.03
L1B	On	55.1	298.5	N.A.	94.8	0.6/1.1	0.90	127	3.11±0.03
L1C	On	80.4	300.5	N.A.	88.4	0.3/1.1	0.71	118	3.35±0.02
L2L1	On	20.4	297.0	123	87.8	0.3/1.7	0.30	120	1.66±0.04
L23	On	55.2	299.3	120	82.3	0.2/1.9	1.79	120	2.54±0.21
L34	On	80.7	298.7	131	78.0	0.2/0.4	0.28	120	5.22±0.19
L45	On	21.0	296.9	130	78.1	0.1/1.35	64.8	60 120	1.70 4.48±0.14
D4	Off	21.3 20.4	296.7 295	122 293	96.8 101.0	0.7 1/1.9	65 4.4	60	0.15834±0.01
L6	On	20.8	297.6	N.A.	90.3	68.7 109.5	1.52	132	1.67 ±0.07
L7	On	21.3	296.9	121	76.8	77.0 110.7	5.79	207	2.78 ±0.12

^a “D” denotes experiments under dark condition. “L” denotes experiments with UV light. The data sets D1-D3 and L1-L4 were obtained and organized from the recent laboratory data reported by Park and Jang (2016). “D” denotes experiments under dark condition. “L” denotes experiments with UV light. Data set D4 was newly added here to estimate the kinetic parameter of heterogeneous autoxidation of SO₂ in the presence of ozone.

^b The accuracy of RH is ±5%. The accuracy of temperature is ±0.5 K.

^c The mass concentration of ATD particles were calculated combining SMPS data, OPC data, the density of dust particles (2.65 g cm⁻³), and the particle size distribution (<3μm). The ppb s associated with the dust particle mass concentration were ±6%.

^d The errors associated with the observation of SO₂, NO, NO₂, and O₃ were ±0.9%, ±12.5%, ±6.9%, and ±0.2%, respectively.

^e The duration is the simulation time from the beginning of the experiment to the end of the experiment.

^f Sulfate concentrations were measured at the end of experiments using PILS-IC. The measurements were not corrected for the particle loss rate to the wall, but corrected for the indigenous sulfate from dust particles.

Table 2. Outdoor chamber experiment condition for SO₂ heterogeneously photooxidation on the ATD particles at variety initial concentration of SO₂, dust particle and NO₂.

Exp. Date	Purpose	RH ^a (%)	Temp. ^a (K)	simulation Time (EST)	Initial Concentration ^b			
					ATD dust ^c ($\mu\text{g m}^{-3}$)	SO ₂ (ppb)	NO/NO ₂ (ppb)	O ₃ (ppb)
28/3/2015	SO ₂	18–67	277.1–301.9	11:10–16:30	N.A.	60.1	0.1/0.9	6.3
	SO ₂ & dust	24–71	277.8–301.5	10:50–16:30	290.1	56.4	0.1/0.7	0.7
16/6/2015	Low dust	15–49	286.7–313.0	8:40–15:30	90.1	100.0	0.1/0.7	0.7
	High dust	16–48	287.0–311.5	9:30–15:30	403.7	120.1	1.1/1.0	5
12/11/2015	Low SO ₂	24–71	277.8–301.5	8:40–17:30	239.2	119.0	0.5/2.0	3.0
	High SO ₂	14–42	296.2–325.0	9:00–17:30	229.0	271.6	0.2/2.1	2.6
26/11/2015	Low NO_x	19–49	288.1–308.6	9:30–15:30	229.6	89.9	19/3.5	10.0
	High NO_x	20–45	288.5–309.1	9:00–15:30	322.3	115.3	70/127.7	3.1
05/11/2016	Low NO_x	26–92	287.0–309.6	9:40–16:15	205.5	39.1	26.4/13.1	5.9
	High NO_x	35–97	287.1–309.4	10:00–16:15	166.6	45.6	49.8/47.8	7.2
22/11/2016	Low NO_x	19–86	275.0–306.5	7:00–15:30	150.3	44.5	14.4/8.7	4.2– 91^d
	High NO_x	26–89	275.2–306.7	7:30–15:30	118.6	44.0	30.2/38.5	5.1– 70^d
<u>14/4/2017</u>	<u>NO_x effect</u>	<u>33–95</u>	<u>287.8–314.3</u>	<u>6:30–17:30</u>	<u>496.2</u>	<u>88.1</u>	<u>88.9/13.5</u>	<u>3.0</u>
<u>25/4/2017–1</u>	<u>NO_x effect</u>	<u>18–89</u>	<u>283.8–313.6</u>	<u>6:00–16:00</u>	<u>414.0</u>	<u>15.0</u>	<u>112.0/13.2</u>	<u>2.2</u>
<u>25/4/2017–2</u>	<u>NO_x effect</u>	<u>26–94</u>	<u>284.1–312.7</u>	<u>6:00–16:00</u>	<u>478.7</u>	<u>17.5</u>	<u>35.9/3.6</u>	<u>1.9</u>

^a The accuracy of RH is $\pm 5\%$. The accuracy of temperature is ± 0.5 K.

^b The errors associated with the observation of SO₂, NO, NO₂, O₃, NH₄⁺ and the concentration of dust particle mass were $\pm 0.9\%$, $\pm 12.5\%$, $\pm 6.9\%$, $\pm 0.2\%$, $5.0\pm\%$ and $\pm 6\%$, respectively. The detailed observations of the chemical species during the experiments were shown in Fig. S4 and Fig. S5 in Supporting Information.

^c The mass concentration of ATD particles were calculated combining SMPS data, OPC data, the density of dust particles (2.65 g cm^{-3}), and the particle size distribution ($<3\mu\text{m}$).

^d ~~30 ppb of isoprene was injected into both chambers to increase the concentration of O₃.~~

Table 3. Dust-phase heterogeneous reactions and their rate constants in the presence of ATD particles.

Reaction ^a	Rate constant ^b	k_1	k_2	k_3	Reference ^b	Note ^c
<i>Partitioning</i>						
1 SO ₂ + Dust → SO ₂ (d) + Dust	d	1×10 ⁻⁸			AR05, HZ15	R7
2 SO ₂ (d) → SO ₂	e	2×10 ⁹	3100	0.013	AR05, HZ15	R8
3 O ₃ + Dust → O ₃ (d) + Dust	d	1×10 ⁻⁸			MU03, US01	
4 O ₃ (d) → O ₃	fe	34 ×10 ¹⁰	2700	<u>0</u>	MU03, US01	
5 NO ₂ + Dust → NO ₂ (d) + Dust	d	1×10 ⁻⁸			CW84	
6 NO ₂ (d) → NO ₂	fe	15 ×10 ¹⁰⁸	2500	<u>0</u>	CW84	
7 HNO ₃ + Dust → HNO ₃ (d) + Dust	d	1×10 ⁻⁸			SW81, Sc84	
8 HNO ₃ (d) → HNO ₃	e	1×10 ¹⁵	8700	15.4	SW81, Sc84	
9 HONO + Dust → HONO(d) + Dust	d	1×10 ⁻⁸			BK96	
10 HONO(d) → HONO	e	1×10 ¹⁰	4900	0	BK96	
11 N ₂ O ₅ + Dust → HNO ₃ (d) + Dust	d	7.3×10 ⁻³			WS09	R20
<i>Dust phase</i>						
1 Dust + $h\nu$ → Dust + e _h	fg	$j_{[ATD]}$			estimated	R10
2 e _h → energy	gh	1×10 ⁻²			estimated	R11
3 e _h + O ₂ → OH(d)	hi	1×10 ⁻²²	2.3		estimated	R12
4 SO ₂ (d) → SO ₄ ²⁻ (d)	gh	5×10 ⁻⁶			estimated	R9
5 SO ₂ (d) + OH(d) → SO ₄ ²⁻ (d)	gh	1×10 ⁻¹²			estimated	R13
6 SO ₂ (d) + O ₃ (d) → SO ₄ ²⁻ (d) + O ₂	gh	2×10 ⁻¹¹			estimated	R14
7 e _h + O ₃ (d) → OH(d) + O ₂	gh	1×10 ⁻¹²			estimated	R15
8 NO ₂ (d) → NO ₃ ⁻ (d)	gh	6×10 ⁻⁵			estimated	R18
9 e _h + NO ₂ (d) → HONO(d)	gh	6×10 ⁻¹²			estimated	R16
10 HONO(d) + $h\nu$ → OH(d) + NO	fg	$j_{[HONO_to_OH]}$				R17
11 NO ₂ (d) + OH(d) → NO ₃ ⁻ (d)	gh	1×10 ⁻¹⁰			estimated	R19
12 NO ₃ ⁻ (d) + Salt(d) → NO ₃ ⁻ (d _{salt})	gh	1×10 ⁻¹²⁸			estimated	
13 SO ₄ ²⁻ (d) + Salt(d) → SO ₄ ²⁻ (d _{salt})	gh	54 ×10 ⁻¹³⁸			estimated	
14 NO ₃ ⁻ (d _{salt}) + SO ₄ ²⁻ (d) → SO ₄ ²⁻ (d _{salt})	gh	41 ×10 ⁻¹³			estimated	

^a The unit of the chemical species (except dust) is molecule cm⁻³ for both partitioning process and the dust phase chemistry. The unit of the dust for model input is mass concentration (μg m⁻³) and is multiplied by a factor of

5 2.45×10¹⁰ for simulation.

^b The rate constant parameters, which are noted as “estimated”, are determined using the simulation of indoor chamber data(Park and Jang, 2016) (see Sect. 3). AR05, Adams et al. (2005); BK96, Becker et al. (1996); CW84, Chameides (1984); HZ15, Huang et al. (2015); MU03, Michel et al. (2003); Sc84, Schwartz (1984); SW81, Schwartz and White (1981); US01, Underwood et al. (2001); WS09, Wagner et al. (2009). The unit of reaction rate constants is s⁻¹ for first-order reactions, cm³ molecule⁻¹ s⁻¹ for second-order reactions (except adsorption reactions).

^c The reactions are noted with the numbers associated with the reaction in main text.

^d Rate constant $k = k_1 \omega f_{\text{dust,M2S}} / 4$, where $\omega = \sqrt{8 R T / (\pi M W)}$ (m s⁻¹) and $f_{\text{dust,M2S}} = 3.066 \times 10^{-6}$ (m² μg). R is the ideal gas constant and MW (g mol⁻¹) is the molecule weight of chemical species.

~~The unit of the rate constants for the sorption reactions is m³-m⁻²-s⁻¹.~~

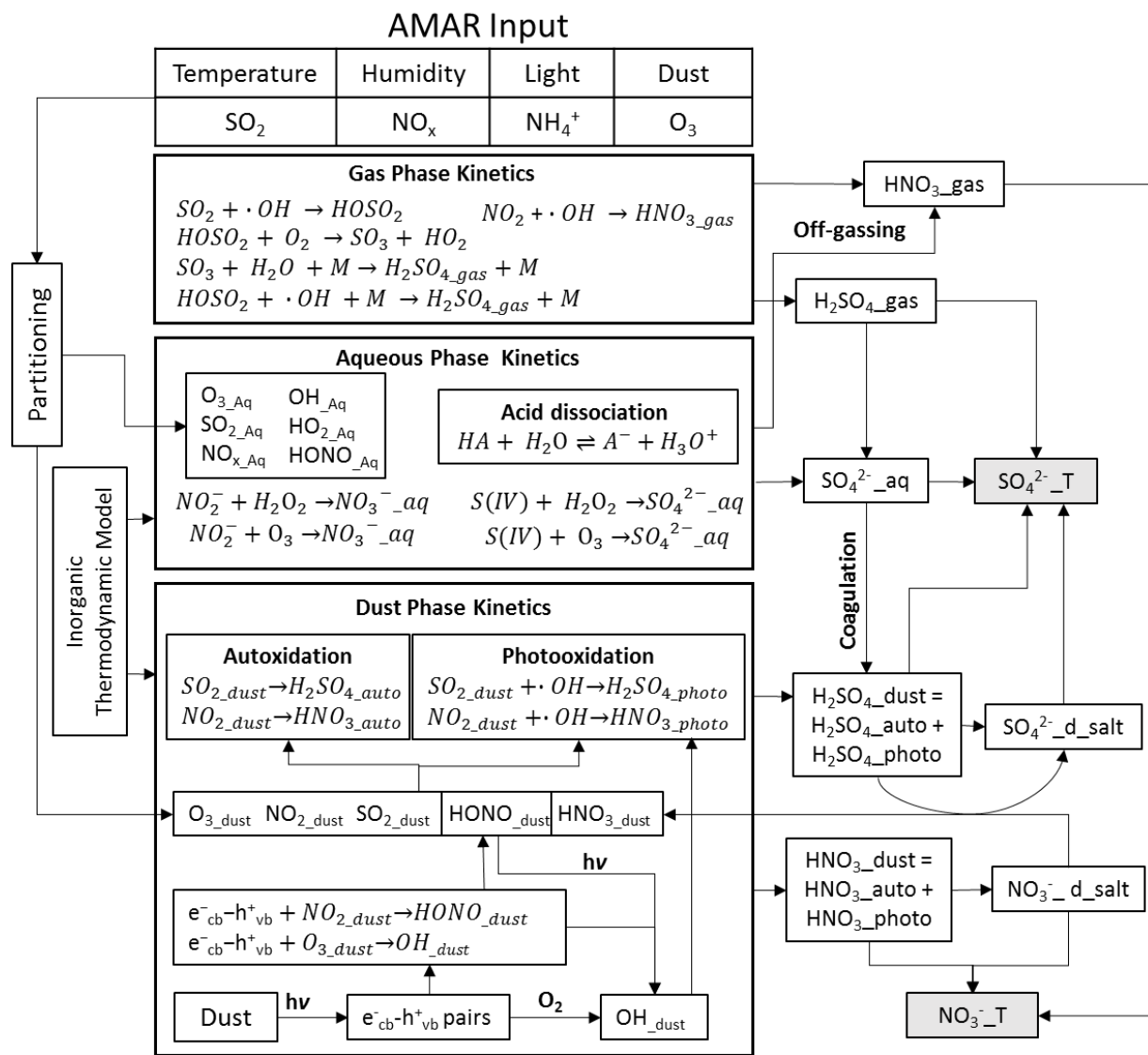
15 ^e Rate constant $k = k_1 \exp\left(-\frac{k_2}{T}\right) / (F_{\text{water}}(1 + k_3/[H^+]))$, where $F_{\text{water}} = \exp(4.4RH) +$

$3.7\exp(4.4RH) \frac{[NO_3^-(d_{\text{salt}})NO_3^-]}{[Dust]} + \frac{M_{\text{in,water}}}{[Dust]}$. [H⁺] and $M_{\text{in,water}}$ are dynamically calculated based on thermodynamic model (E-AIM II) (Clegg et al., 1998;Wexler and Clegg, 2002;Clegg and Wexler, 2011).

~~^f Rate constant $k = k_{\text{f}} \exp\left(-\frac{k_{\text{f}}}{T}\right)$.~~

^{fe} Photocatalytic reaction. The cross sections and quantum yields of dust are estimated (see Sect. 2.2). The cross sections and quantum yields of HONO(d) are taken from Bongartz et al. (1991) and Atkinson et al. (1997), respectively.

^{hg} Rate constant $k = k_1$. ^{hf} Rate constant $k = k_1 \exp(k_2)$.



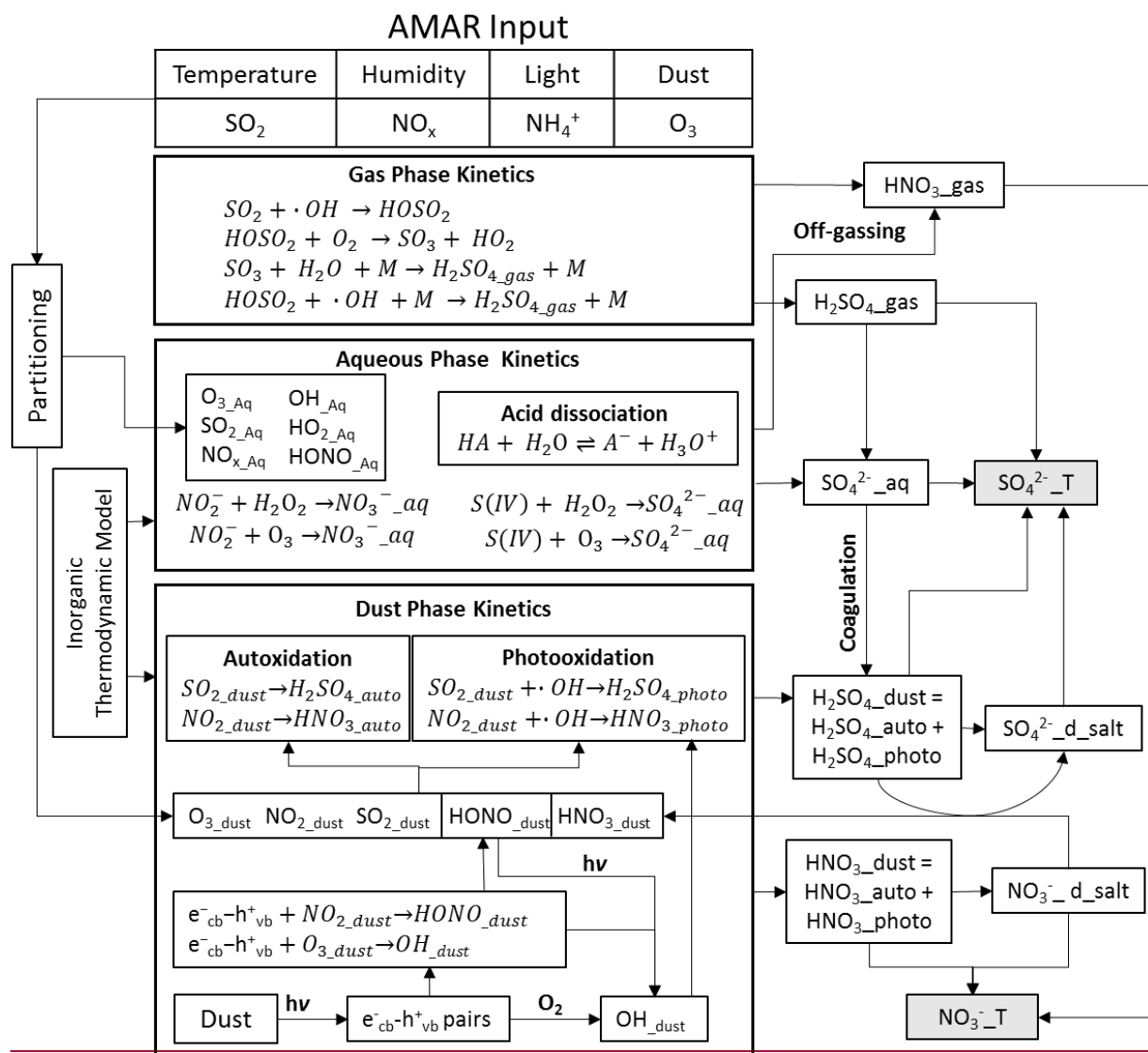


Figure 1. The overall schematic of the AMAR model to simulate heterogeneous SO₂ oxidation. For the description of chemical species, gas phase, aqueous phase and dust phase are symbolized as “gas”, “aq” and “dust”, respectively. SO₄²⁻_T, H₂SO₄_{gas}, SO₄²⁻_{aq} and H₂SO₄_{dust} are the total sulfate formation and the formation of sulfate from gas phase, aqueous phase and dust phase, respectively. SO₄²⁻_{d_salt} and NO₃⁻_{d_salt} are the neutralized sulfate and nitrate in dust phase.

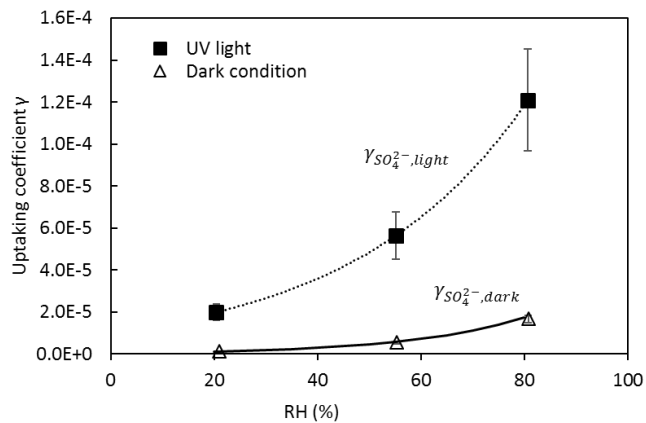


Figure 2. Uptake coefficient (γ) of SO_2 in the presence of the ATD particles under dark condition and UV light condition. The values of γ were obtained by kinetic model using indoor
5 experimental data. The $\gamma_{\text{SO}_4^{2-}, \text{light}}$ is correlated to concentration of OH radicals and RH (%). The $\gamma_{\text{SO}_4^{2-}, \text{dark}}$ is a function of RH. The error bar of γ was derived from the model uncertainty.

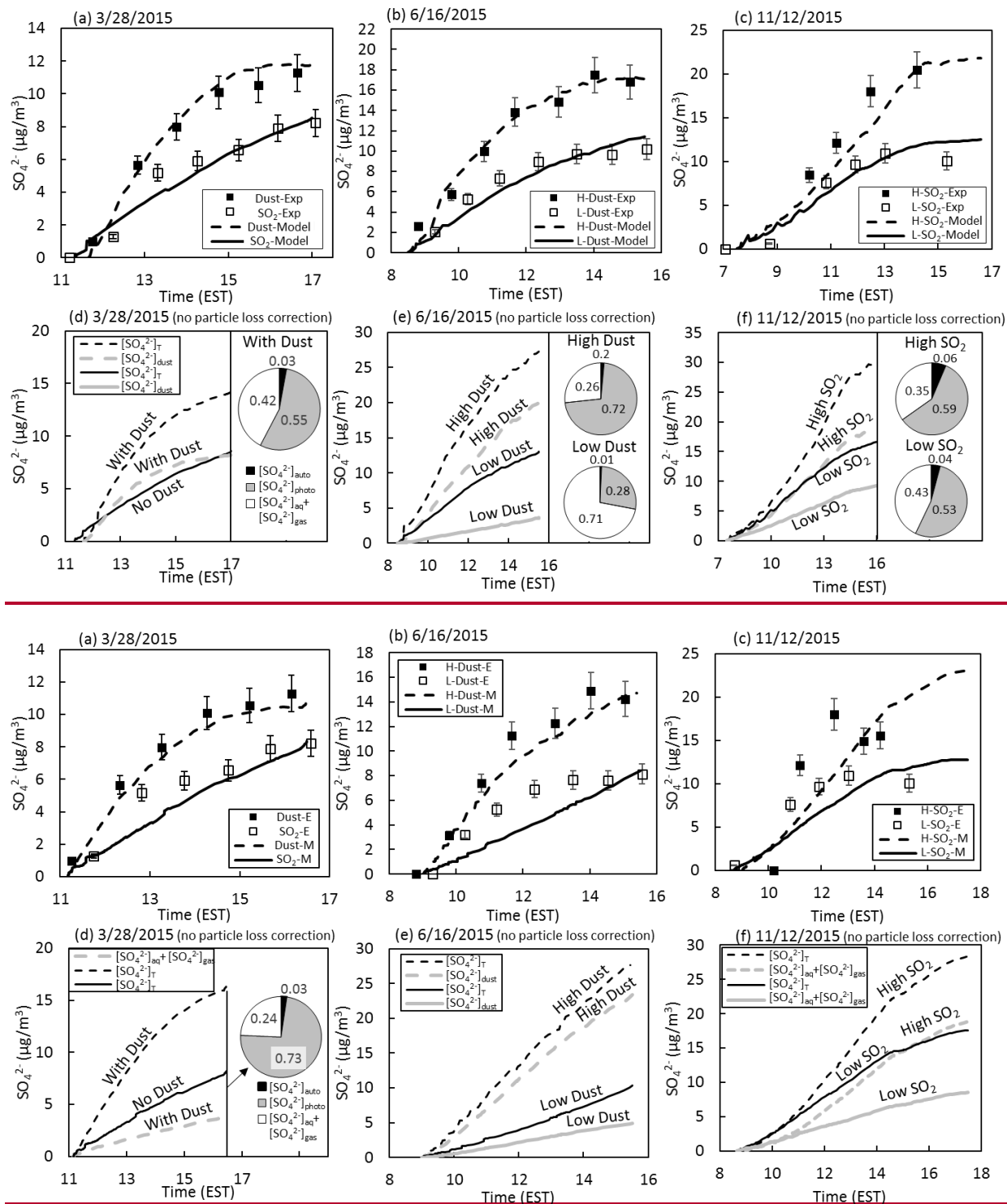


Figure 3. Time profiles of total sulfate concentration (SO_4^{2-} , $\mu\text{g m}^{-3}$) in the UF-APHOR. “Exp” denotes the experimentally observed sulfate ($[\text{SO}_4^{2-}]_{\text{T}}$) and “Model” denotes the model-predicted sulfate. ~~Sulfate concentrations were measured using PILS-IC during the experiments. The “H” and “L” represent the high and the low initial concentrations of chemical species.~~ The errors

associated with the concentration of sulfate is $\pm 10\%$ originated from the PILS–IC measurement.

(a) Sulfate formation with and without ATD particles (SO_2 60 ppb vs. SO_2 56 ppb and dust $290 \mu\text{g m}^{-3}$).

(b) The high and low loadings of dust particles (dust $90 \mu\text{g m}^{-3}$ and SO_2 100 ppb vs. dust $404 \mu\text{g m}^{-3}$ and SO_2 120 ppb).

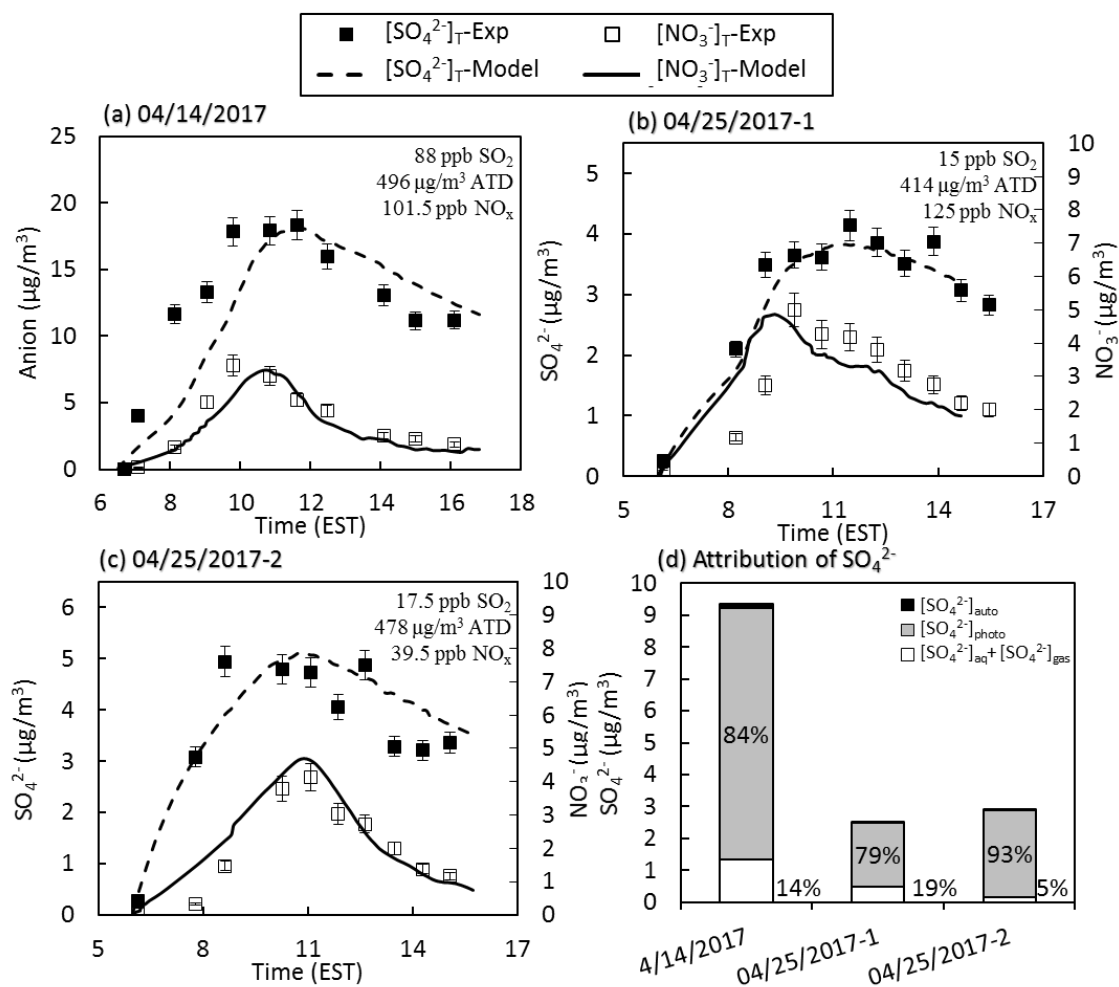
(c) The high and the low concentrations of SO_2 (SO_2 119 ppb and dust $239 \mu\text{g m}^{-3}$ vs. SO_2 272 ppb and dust $230 \mu\text{g m}^{-3}$).

5 For Fig. 3(a), 3(b) and 3(c), the simulations included the chamber dilution and the wall process of gaseous compounds and particles (Sect. S1).

For Fig. 3(d), 3(e) and 3(f), the wall process for the particle loss was excluded to estimate the influence of ATD particles on sulfate formation without the chamber artefacts.

In Fig. 3(d), 3(e) and 3(f), total sulfate was decoupled into the sulfate originated from dust chemistry ~~and that~~

10 ~~originating from non-dust chemistry~~ ($[\text{SO}_4^{2-}]_{\text{dust}} = [\text{SO}_4^{2-}]_{\text{photo}} + [\text{SO}_4^{2-}]_{\text{gas auto}}$). The pie charts inserted into Fig. 3(d), 3(e) and 3(f) illustrates how total sulfate is attributed to major pathways at the end of the experiments.



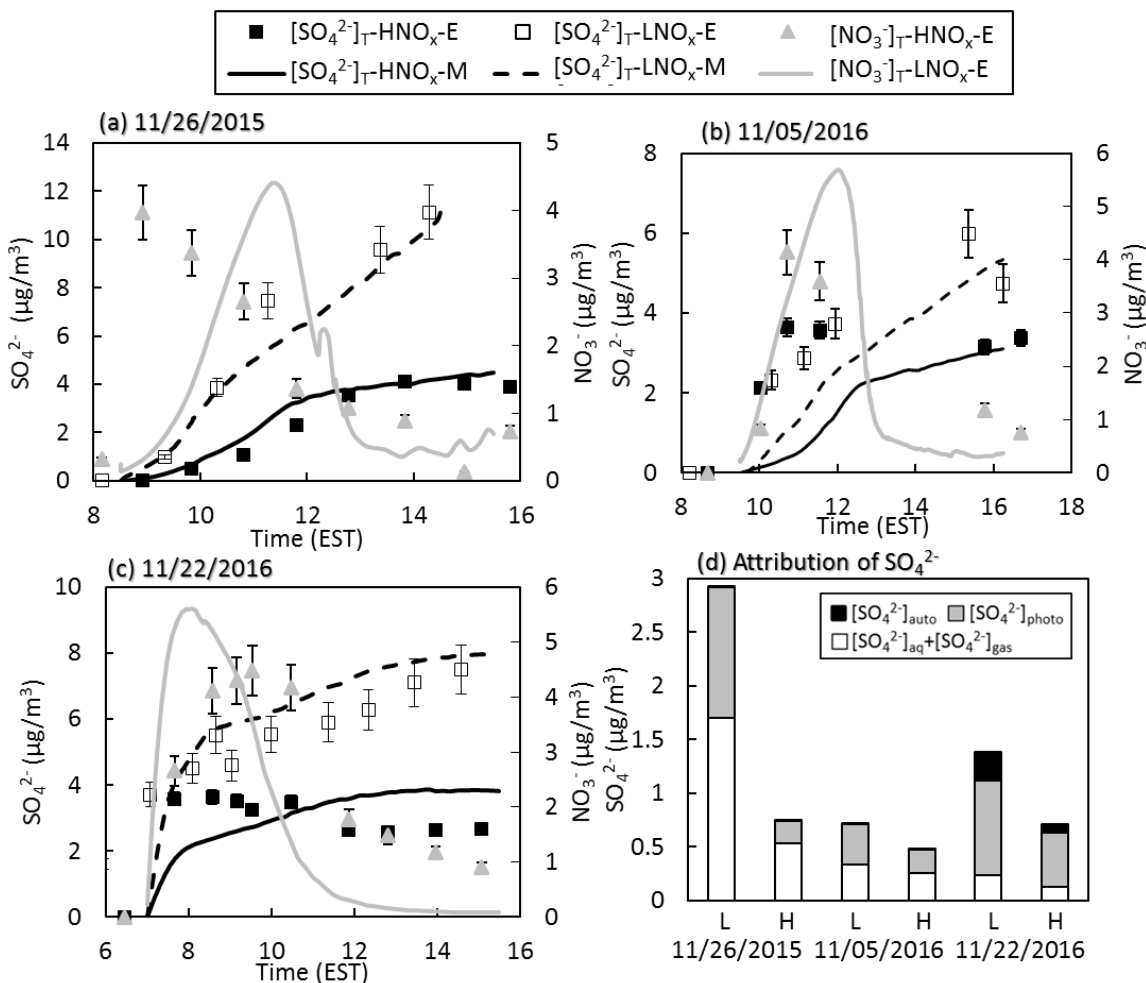


Figure 4. Time profiles of total sulfate concentration ($[\text{SO}_4^{2-}]_{\text{T}}$, $\mu\text{g}/\text{m}^3$) and nitrate concentration ($[\text{NO}_3^-]_{\text{T}}$, $\mu\text{g}/\text{m}^3$) in the dual chamber experiments using UF-APHOR at the two different NO_x

levels. The concentrations of sulfate and nitrate were measured using PILS-IC during the experiments. The error bars of the concentration of sulfate and nitrate is $\pm 10\%$ originated from the PILS-IC measurement. The detailed experimental conditions of Fig. 4(a) (SO_2 90 ppb, NO_x 23 ppb and dust $230 \mu\text{g}/\text{m}^3$ vs. SO_2 115 ppb, NO_x 198 ppb and dust $322 \mu\text{g}/\text{m}^3$), Fig. 4(b) (SO_2 39 ppb, NO_x 40 ppb and dust $206 \mu\text{g}/\text{m}^3$ vs. SO_2 46 ppb, NO_x 98 ppb and dust $167 \mu\text{g}/\text{m}^3$), and Fig. 4(c) (SO_2 45 ppb, NO_x 23 ppb and dust $150 \mu\text{g}/\text{m}^3$ vs. SO_2 44 ppb, NO_x 69 ppb and dust $119 \mu\text{g}/\text{m}^3$) are shown in Table 2. Figure 4(d) shows how total sulfate is attributed to aqueous phase reaction (sulfate formation in gas phase + sulfate formation in inorganic salted inorganic aqueous phase) ($[\text{SO}_4^{2-}]_{\text{aq}} + [\text{SO}_4^{2-}]_{\text{gas}}$), dust-phase autoxidation ($[\text{SO}_4^{2-}]_{\text{auto}}$), and dust photochemistry ($[\text{SO}_4^{2-}]_{\text{photo}}$) at the end of the experiments. For Fig. 4(c), 30 ppb of isoprene was injected to both chambers to yield a high concentration of ozone (90 ppb). “Exp” denotes the experimental observation and “Model” denotes the simulation using the AMAR module. “H” and “L” represent the high and low initial concentration of NO_x within the one set of dual chamber experiment. The chamber dilution and the wall process of gaseous compounds and particles were included in the simulation (Sect. S1).

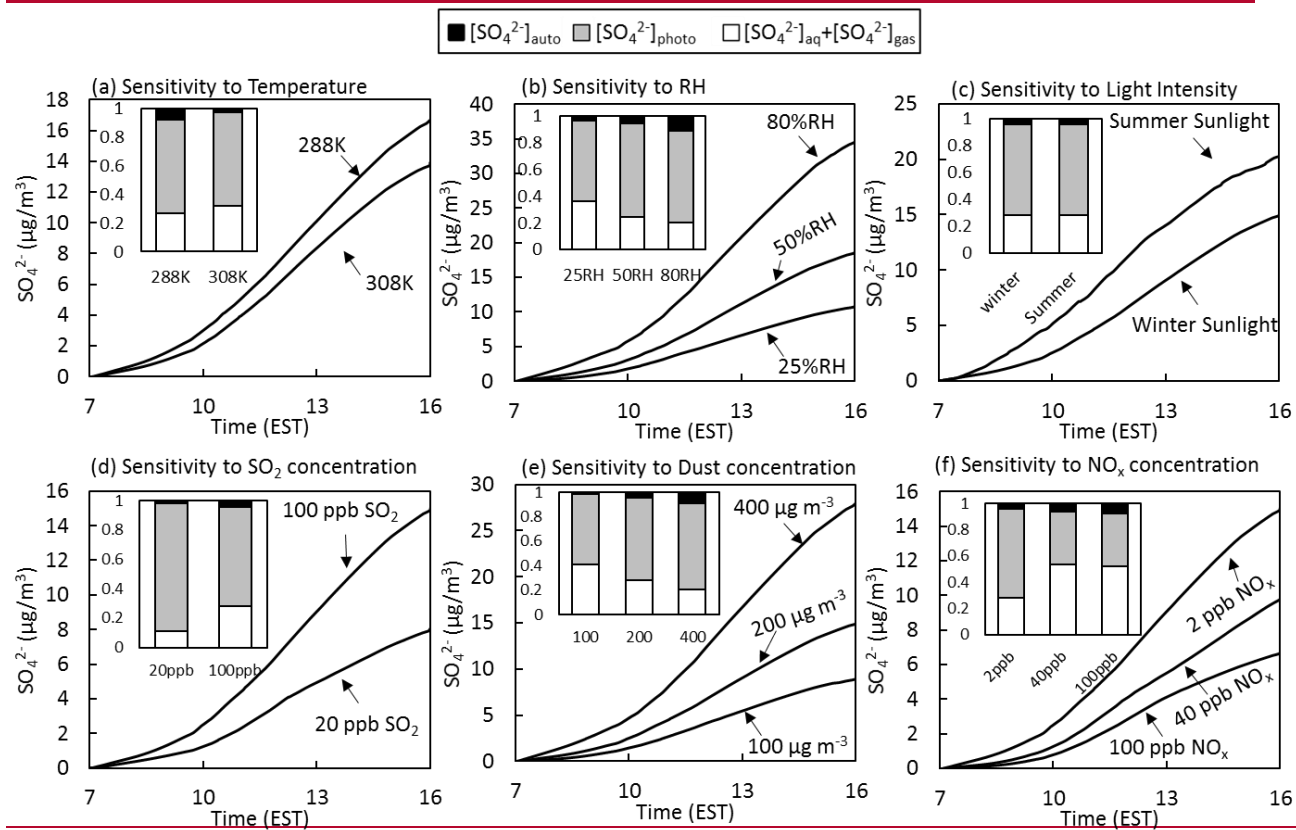
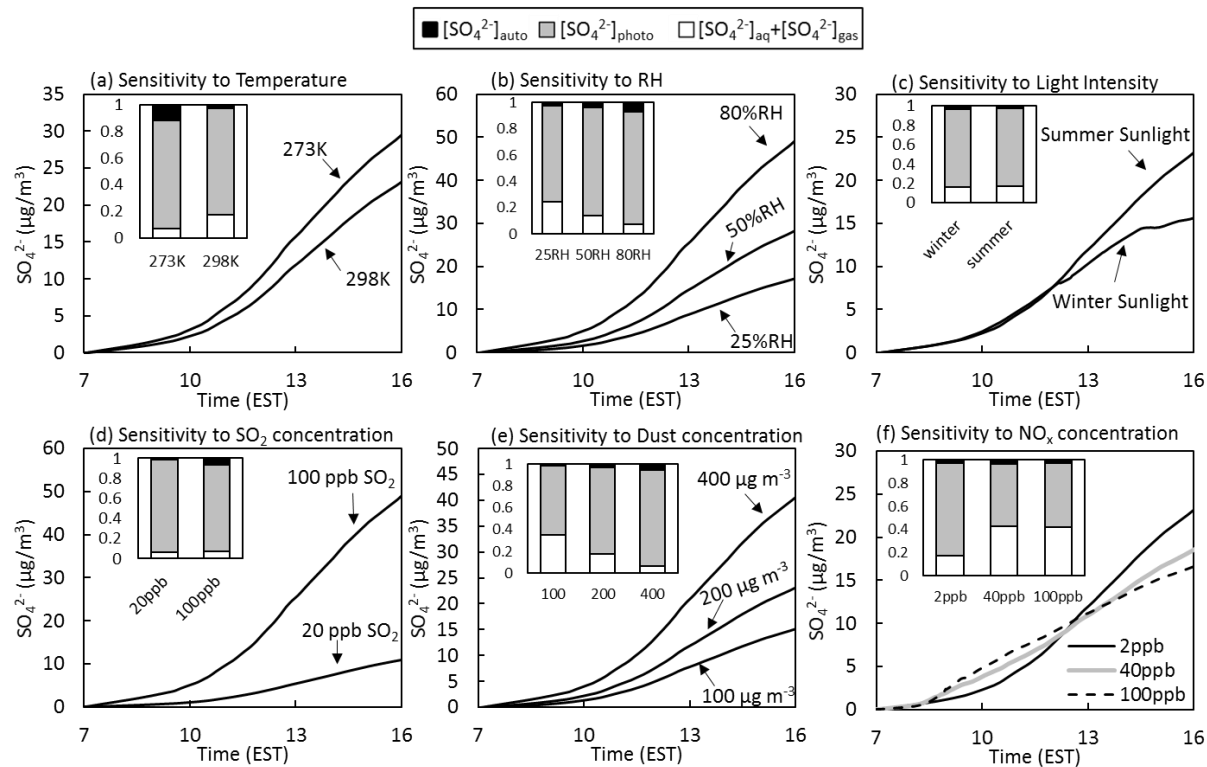


Figure 5. Sensitivity test of AMAR model to (a) temperature at ~~288K-273K~~ and ~~29308K~~; (b) RH at 25%, 50% and 80%; (c) sunlight profiles of summertime (~~11-May25 April, 2017~~) and

wintertime (~~22~~12 November, ~~2015~~6) at Gainesville, Florida (latitude/longitude: 29.64185°/–82.347883°); (d) the concentration of SO₂; (e) the concentration of dust particles; and (f) the NO_x concentration (initial NO:NO₂=1:1). The stacked column chart in each figure illustrates how total sulfate is attributed to major pathways at the end of each experiment. For the sensitivity test, the chamber simulation is conducted with 100 ppb of initial SO₂, 2 ppb of initial NO₂, 2 ppb of initial O₃ and 200 μg m⁻³ of ATD particles at T = 298K and RH = 40% under ambient sunlight on ~~22-25 November-April 2016~~2017. NO_x (rate of flux = 2.7×10⁶, s⁻¹) and isoprene (rate of flux = 2.7×10⁶, s⁻¹) were constantly added to simulate chamber dilution. The simulation was performed without considering the particle loss to the chamber wall.

10